# Seasonal modeling analysis of nitrate formation pathways in Yangtze River Delta region, China

Jinjin Sun[1,2], Momei Qin[1*], Xiaodong Xie[1], Wenxing Fu[1], Yang Qin[1,2], Li Sheng[1], Lin Li[1], Jingyi Li[1], Ishaq Dimeji Sulaymon[1], Lei Jiang[1], Lin Huang[1], Xingna Yu[2], Jianlin Hu[1*]

[1] Jiangsu Key Laboratory of Atmospheric Environment Monitoring and Pollution Control, Collaborative Innovation Center of Atmospheric Environment and Equipment Technology, Nanjing University of Information Science & Technology, Nanjing 210044, China

[2] Key Laboratory of Meteorological Disaster, Ministry of Education, Joint International Research Laboratory of Climate and Environment Change, Collaborative Innovation Center on Forecast and Evaluation of Meteorological Disasters, Key Laboratory for Aerosol-Cloud-Precipitation of China Meteorological Administration, Nanjing University of Information Science and Technology, Nanjing 210044, China


*Correspondence to:* Jianlin Hu (jianlinhu@nuist.edu.cn) and Momei Qin (momei.qin@nuist.edu.cn)

## Abstract

Nitrate ($NO_3^-$) has been the dominant and the least reduced chemical component of fine particulate matter ($PM_{2.5}$) since the stringent emission control implemented in China in 2013. The formation pathways of $NO_3^-$ vary seasonally and differ substantially in daytime vs. nighttime. They are affected by precursor emissions, atmospheric oxidation capacity, and meteorological conditions. Understanding $NO_3^-$ formation pathways provides insights for the design of effective emission control strategies to mitigate $NO_3^-$ pollution. In this study, the Community Multiscale Air Quality (CMAQ) model was applied to investigate the impact of regional transport, predominant physical processes, and different formation pathways to $NO_3^-$ and total nitrate ($TNO_3$, i.e., $HNO_3+NO_3^-$) production in the Yangtze River Delta (YRD) region during the four seasons of 2017. $NO_3^-/PM_{2.5}$ and $NO_3^-/TNO_3$ are the highest in the winter, reaching 21% and 94%, respectively. Adjusted gas ratio (adjGR = $([NH_3] + [NO_3^-])/([HNO_3] + [NO_3^-])$) in YRD is generally greater than two in different seasons across most areas in YRD, indicating that YRD is mostly in the $NH_3$-rich regime and $NO_3^-$ is limited by $HNO_3$ formation. Local emissions and regional transportation contribute to YRD $NO_3^-$ concentrations by 50–62% and 38–50%, respectively. Majority of the regional transport of $NO_3^-$ concentrations is contributed by indirect transport (i.e., $NO_3^-$ formed by transported precursors reacting with local precursors). Aerosol (AERO, including condensation, coagulation, new particle formation and aerosol growth) processes are the dominant source of $NO_3^-$ formation. In summer, $NO_3^-$ formation is dominated by AERO and total transport (TRAN, sum of horizontal and vertical transport) processes. The $OH+NO_2$ pathway contributes to 60–83% of the $TNO_3$ production, and the $N_2O_5$ heterogeneous (HET $N_2O_5$) pathway contributes to 10–36% in YRD. HET $N_2O_5$ contribution becomes more important in cold seasons than warm seasons. Within the planetary boundary layer in Shanghai, the $TNO_3$ production is dominated by the $OH+NO_2$ pathway during the day (98%) in the summer and spring, and by the HET

$N_2O_5$ pathway during the night (61%) in the winter. Local contribution dominates the OH+$NO_2$ pathway for $TNO_3$ production during the day, while indirect transport dominates the HET $N_2O_5$ pathway at night.

*Keywords:* Nitrate formation pathways; chemical transport model, process analysis; local and transport contributions; Yangtze River Delta.

## *1. Introduction*

The Yangtze River Delta (YRD) region, located in eastern China, is among the most populous and developed economic regions in China. Because of rapid population growth, economic advancement, urbanization, and industrialization during recent decades, the YRD region has been frequently suffering from both fine particulate matter ($PM_{2.5}$) and ozone ($O_3$) pollution problems (Qin et al., 2021;Sun et al., 2019;Dai et al., 2021). Particulate nitrate ($NO_3^-$) is a major $PM_{2.5}$ component and high concentrations of $NO_3^-$ are often observed during cold seasons in the YRD region, due to high precursors emissions and regional transport contribution. Huang et al. (2014) reported that the daily average $PM_{2.5}$ concentrations in Shanghai were 91 μg m$^{-3}$ during haze pollution events of 5–25 January 2013, whereas $NO_3^-$ accounted for 14% total $PM_{2.5}$ mass. Huang et al. (2020a) observed that $PM_{2.5}$ concentrations in Nanjing were 271 μg m$^{-3}$ on 30–31 December of 2017, and the fraction of $NO_3^-$ was ~27%. Lin et al. (2020) found that the peak concentration of $NO_3^-$ in Nanjing was 85 μg m$^{-3}$ during haze pollution events in the spring of 2016.

Owing to the stringent emission control strategies implemented in China since 2013, $PM_{2.5}$, sulfur dioxide ($SO_2$) and nitrogen oxides ($NO_x$ = nitric oxide (NO) + nitrogen dioxide ($NO_2$)) emissions have decreased substantially, which led to significant decreases in primary $PM_{2.5}$ and sulfate ($SO_4^{2-}$) concentrations in China (Li et al., 2022;Chen et al., 2021). However, compared to $SO_4^{2-}$ and other $PM_{2.5}$

Atmospheric
Chemistry
and Physics
Discussions

Open Access

EGU

components, the reduction rate of $NO_3^-$ was much less slower (Wen et al., 2018;Zhai

75          et al., 2021;Zhou et al., 2022;Wang et al., 2022). This led to a rise in the ratio of

$NO_3^-$ mass to total $PM_{2.5}$ in eastern China, rendering $NO_3^-$ the dominant chemical

component of $PM_{2.5}$ (accounting for 24–35 %, especially during the cold season and

haze pollution events) (Ding et al., 2019;Wen et al., 2018;Lin et al., 2020;Fu et al.,

2020;Zhou et al., 2022). High concentrations of $NO_3^-$ influence the hygroscopicity

80          and optical properties of particles, contributing to the formation of haze and to

visibility degradation (Hu et al., 2021;Xie et al., 2020). Mitigating $NO_3^-$ pollution has

become an urgent concern in YRD.

$NO_3^-$ is formed in the atmosphere by a series of chemical reactions leading to the

production of nitric acid ($HNO_3$) and then following gas-to-particle partitioning

85          (Griffith et al., 2015;Guo et al., 2018;Lin et al., 2020). The key $NO_3^-$ formation

pathways include the gas-phase oxidation (hydroxyl (OH) and $NO_2$) and the

heterogeneous hydrolysis of dinitrogen (HET $N_2O_5$) on the wet particles' surface (Fan

et al., 2021;Wang et al., 2018;Chen et al., 2020). Several studies investigated the

importance of different pathways to $NO_3^-$ formation in various locations using

90          chemical transport models (CTMs), field observations, the box model, or oxygen and

nitrogen isotope techniques. For example, He et al. (2020) and Li et al. (2021b)

reported that the $OH+NO_2$ pathway dominates daytime $NO_3^-$ formation in the YRD,

accounting for 60–92 % and 55–86 % in warm and cold seasons, respectively. The

HET $N_2O_5$ pathway is the main nocturnal-$NO_3^-$ formation in winter, especially in

95          severe haze episodes, with contributions of 44–97 % at night (Fu et al., 2020;He et al.,

2018). Furthermore, Tan et al. (2021) and Wang et al. (2018) indicated that the

chemical formation cannot explain the variation of $TNO_3$ at the surface (sum of $NO_3^-$

and $HNO_3$), due to the concentrations of $N_2O_5$ being close to zero and controlled by

high NO emissions at night. Fan et al. (2021) and Kim et al. (2014) further emphasized

100         the contributions of $NO_3^-$ formation pathways differ significantly at vertical altitudes,

Atmospheric
Chemistry
and Physics
Discussions
Open Access
EGU

owing to the vertical gradients of nocturnal $NO_3$ and total oxidant ($NO_2+O_3$) level within the planetary boundary layer (PBL). Prabhakar et al. (2017) revealed that the active nocturnal $NO_3^-$ formation via the HET $N_2O_5$ pathway from the upper PBL contributed to daytime surface $NO_3^-$ concentrations in California, accounting for 80 %.

105      The complex $NO_3^-$ formation chemistry involves the anthropogenic emission of precursors (i.e., $NO_x$, and ammonia ($NH_3$)) and atmospheric oxidants (i.e., OH, $O_3$, and $N_2O_5$) (Chan et al., 2021;Womack et al., 2019). Studies suggested that $NO_3^-$ responds nonlinearly to its precursors emissions reductions in major Chinese regions (i.e., the North China Plain (NCP) and YRD), emphasizing that the uncoordinated

110      control of precursors (i.e., $SO_2$, $NH_3$, and $NO_x$) increase the atmospheric oxidant capacity (AOC) and enhance $NO_3^-$ formation in $NO_x$-rich regimes (Li et al., 2021b;Huang et al., 2020b;Lu et al., 2021a). Coupled with the chemical formation, regional transport also plays important roles in $NO_3^-$ pollution formation. Previous modeling studies using the CTMs highlighted the important role of the regional

115      transport in $NO_3^-$ concentrations in major regions of eastern China (Itahashi et al., 2017;Qu et al., 2021;Ying et al., 2014;Shen et al., 2020). For example, Huang et al. (2020a) reported that secondary pollutants are regionally transported between the NCP and YRD regions (a distance of 1000 km), and hence simultaneously exacerbate the levels of secondary inorganic aerosols (SIA) in two major Chinese regions. Ying et al.

120      (2014) revealed that the regional air pollution transport from the north and central China contributed about 45 % to $NO_3^-$ in Shanghai during the winter of 2009. Wu et al. (2017) suggested that the regional transport plays a key role in $NO_3^-$ sources in Shanghai (accounting for about 90 %), while local emission only contributed 10 % for $NO_3^-$ in January 2013. Shen et al. (2020) reported that the contribution of regional

125      transport amounted to around 60–98 % to the high concentrations of $NO_3^-$ under severe haze episodes in two winters of 2015 and 2016 in the YRD. Qu et al. (2021) found that the indirect transport made a contribution of 43 % to $NO_3^-$ in the Pearl River Delta

(PRD) region in cold season of 2015, mainly due to chemical reactions between the locally emitted NOx and transported $O_3$ at night. Du et al. (2020) also revealed that

130    regional transport contributed about 56 % to $NO_3^-$ in Beijing in winter 2017, mainly produced via indirect transport.

     The $NO_3^-$ formation pathways and controlling factors can be very different in different seasons even in the same studying region. Most previous studies on $NO_3^-$ focused on one or a few short period of pollution episodes, but lack of seasonal

135    analysis. This study aims to obtain a comprehensive understanding of the seasonal variations in the $NO_3^-$ formation mechanisms, as well as to determine key precursors, dominant processes and chemical pathways in YRD. The Community Multiscale Air Quality (CMAQ) model was employed to investigate the contributions of various physical and chemical processes to $NO_3^-$ and $HNO_3$ formation. Regional transport and

140    chemical reaction pathways were quantified for the YRD region. The analyses were conducted in the four seasons of 2017 to compare and identify the key impact factors for $NO_3^-$ in different seasons, and to provide a scientific basis for designing effective emissions control strategies to mitigate the urgent $NO_3^-$ pollution in the YRD region.

## *2. Methods*

145    *2.1. Model configuration*

     The CMAQ v5.2 model (Wyat Appel et al., 2018;Liu et al., 2020b;Sheng et al., 2022) was applied to investigate the major chemical pathways and physical processes that contribute to $NO_3^-$ and $TNO_3$ formation in the YRD region. Two nested domains were used, as shown in Fig. 1. The outer domain (36 km horizontal resolution) spanned

150    eastern and southeastern China, while the inner domain (12 km horizontal resolution) spanned the entire YRD region. The simulation periods were January, April, July, and October 2017, representing the winter, spring, summer, and autumn, respectively. The simulation began three days prior to each of the study periods, and the results were not

included in the model analysis as they served as a spin-up of the model.

155     The CMAQ model was configured using the photochemical mechanism of the State-wide Air Pollution Research Center version 07 (SAPRC07tic) and the sixth-generation aerosol (AERO6i) module (Fu et al., 2020;Sulaymon et al., 2021). Further details about the CMAQ modeling system provided in previous studies (Hu et al., 2016;Liu et al., 2020b). The Weather Research and Forecasting model (WRF v4.2,

160     http://www.wrf-model.org) was used to simulate the required meteorological fields inputs, with initial and boundary meteorological conditions from the 1°×1° National Centers for Environmental Prediction Final (NCEP/FNL) reanalysis data (https://rda.ucar.edu/datasets/ds083.2/). Detailed configurations of the WRF model provided in the studies of Hu et al. (2016) and Wang et al. (2021), shown in Table S1,.

165     The anthropogenic emissions of 2017 in the YRD region were released by the Shanghai Academy of Environmental Sciences (SAES) (An et al., 2021), and used for the entire YRD region. The Multi-resolution Emission Inventory for China of the year 2017 with resolution of 0.25° × 0.25° (MEIC v1.3, http://meicmodel.org) served as the anthropogenic emissions for other Chinese regions outside the YRD (Zheng et al.,

170     2018). Emissions from other regions outside China in the inner domain were calculated using the gridded Regional Emission inventory in ASia (REAS v3.2, 0.25° × 0.25° resolution) emissions of the year 2015. The global model of emissions of gases and aerosols from nature (MEGAN v2.1) was used to estimate biogenic emissions (Guenther et al., 2012). Biomass burning emissions were based on satellite observations

175     including both gases and aerosols from the 2017 Fire Inventory from NCAR (FINN) (Wiedinmyer et al., 2011). Further descriptions of the emissions processing are provided in previous studies by Hu et al. (2016) and Qiao et al. (2015), and therefore not repeated here.

*2.2. Contributions of transport*

180     To quantify the contributions of local and regional transport to the surface

Atmospheric
Chemistry
and Physics
Discussions

Open Access

EGU

concentrations of the nitrate-phase species (i.e., $HNO_3$ and $NO_3^-$), four scenarios were simulated under the same meteorological fields. Briefly, in the first (base) scenario, the anthropogenic emissions of 2017 in the YRD and outside regions were included. In the second (YRD-zero) scenario, anthropogenic emissions in the YRD were set to zero, while anthropogenic emissions in regions outside YRD were used. In the third (outside-zero) scenario, only anthropogenic emissions in the YRD were included, while the regions outside the YRD were set to zero. The fourth (all-zero) scenario represented the background case, where the anthropogenic emissions within the study domain were set to zero.

The predicted concentrations were denoted as $C_{base}$, $C_{YRD-zero}$, $C_{outside-zero}$, and $C_{all-zero}$, representing concentration associated with the base, YRD-zero, outside-zero, and all-zero scenarios, respectively. For $NO_3^-$ in YRD, the contributions of local YRD emissions, direct transport ($NO_3^-$ contributed by transported precursors from outside regions), indirect transport ($NO_3^-$ contributed by transported and local-emitted precursors), and background were defined as $F_{Local}$, $F_{Direct}$, $F_{Indirect}$, and $F_{Background}$, and they were quantified as follows:

$$F_{Local} = (C_{outside-zero} - C_{all-zero})/C_{base} \qquad (1)$$

$$F_{Direct} = (C_{YRD-zero} - C_{all-zero})/C_{base} \qquad (2)$$

$$F_{Indirect} = [(C_{base} - C_{outside-zero}) - (C_{YRD-zero} - C_{all-zero})]/C_{base} \qquad (3)$$

$$F_{Background} = C_{all-zero}/C_{base} \qquad (4)$$

In addition to $NO_3^-$, the major gases (i.e., $O_3$, $NH_3$, $NO_2$, and $HNO_3$), atmospheric oxidants (i.e., OH, and $N_2O_5$) and particulate pollutants ($PM_{2.5}$, $SO_4^{2-}$, and SOC) were also quantified. The values of the contributions of the local, direct and indirect transport emissions can be greater or less than zero, which represents the generation or depletion of pollutants through chemical reactions between local and non-local precursors.

*2.3. Process analysis*

In the CMAQ model system, the process analysis (PA) tool has two components,

including the Integrated Process Rate (IPR) and Integrated Reaction Rate (IRR) (Liu et al., 2011;Byun and Schere, 2006). The IPR analysis was applied to investigate the

210 cumulative effect of chemical and physical processes to $NO_3^-$ and $HNO_3$ formation and their daily variation within the PBL (Chen et al., 2019;Yang et al., 2020;Kim et al., 2014). These processes, as explained in Table S2, include aerosol processes (AERO), gas chemistry (CHEM), emission (EMIS), horizontal transport (HTRA), vertical transport (VTRA), dry deposition (DDEP), and cloud processes (CLDS). Furthermore,

215 the IRR analysis was employed to quantify the rates of $TNO_3$ chemical reactions pathways (Qu et al., 2021;Fu et al., 2020;Shen et al., 2020). The complex chemical production of $TNO_3$ involves eight reactions pathways, detailed in Table S3 (Qu et al., 2021;Fu et al., 2020;Chuang et al., 2022). In the latter analyses, these pathways are grouped into three major $TNO_3$ production pathways, including the $OH+NO_2$, HET

220 $N_2O_5$, and "Others" pathways, according to their importance. Shanghai is selected as an example in the IPR and IRR analysis to explore the impacts of physical and chemical processes of $NO_3^-$ and $HNO_3$ formation because it is the largest city in YRD and has the most abundant measurement data.

*2.4. Observation data*

225 Hourly concentrations of six routine air pollutants (i.e., $O_3$, $PM_{2.5}$, $NO_2$, $SO_2$, and carbon monoxide (CO)) in five representative YRD cities (i.e., Shanghai, Nanjing, Hefei, Hangzhou, and Changzhou, shown in Fig. 1) during the four seasons were obtained from the China Ministry of Ecology and Environment (http://106.37.208.233:20035/, last accessed on April 30, 2022). Furthermore, hourly

230 $NO_3^-$ concentrations were measured by the Monitors for AeRosols and Gases (MARGA 1S ADI 2080, Netherlands) (Khezri et al., 2013) at four urban atmospheric environment supersites, including Shanghai (31.23°N, 121.54°E), Hefei (31.78°N, 117.20°E), Hangzhou (30.29°N, 120.16°E), and Changzhou (31.76°N, 119.96°E). Observation data of meteorological parameters (temperature (T2, °C), relative humidity (RH, %),

235    wind speed (WS, m/s) and wind direction (WD, °)) for 75 weather stations in YRD were downloaded from the Chinese Meteorological Agency (http://data.cma.cn/en, last accessed on November 30, 2021).

       The statistical metrics used for the WRF-CMAQ model evaluation include the mean bias (MB), normalized mean bias (NMB), normalized mean error (NME),

240    correlation coefficient (R), root mean square error (RMSE), and index of agreement (IOA). Definitions and criteria of all statistical metrics are illustrated in Table S4. The benchmarks of major air pollutants ($PM_{2.5}$, $NO_2$, $O_3$, and $NO_3^-$) concentrations are suggested by Emery et al. (2017) and Huang et al. (2021). The benchmarks of major meteorological parameters (T2, WS, and WD) are suggested by Emery and Tai (2001).

245    ***3. Results and discussion***

### 3.1. Model evaluation

#### 3.1.1. WRF model performance

       Table 1 shows the modeling performance statistics of the meteorological parameters in the four seasons of 2017. Predicted T2 and WS values are slightly higher than the observations, and MB values of T2 and WS exceed the suggested benchmark

250    (MB ≤ ±0.5) in all seasons. The seasonal and annual IOA values of T2 occur within the suggested benchmark (IOA ≥ 0.8). For WS, the seasonal and annual values of RMSE and IOA all meet the suggested criterion (RMSE ≤ 2.0 and IOA ≥ 0.6). The MB values of WD are slightly above the suggested benchmark (MB ≤ ±10) in the four seasons,

255    except during spring. RH is generally under-estimated compared to the observations with averaged MB values of –6.96, –10.7, –9.06, and –5.98 in winter, spring, summer, and autumn, respectively. No suggested criterion for MB value of RH. In addition, high seasonal and annual values of R (0.85–0.95 for T; 0.87–0.91 for RH; 0.70–0.85 for WS; and 0.75–0.89 for WD) are found. The WRF performance in this study is comparable

260    to WRF performance in previous studies (Wang et al., 2021;Hu et al., 2016;Sulaymon

et al., 2021).

### 3.1.2. CMAQ model performance

Table 2 and Fig. S1 show the model performance and time series of major air pollutants in the four seasons. Overall, the CMAQ model has reasonably reproduced

265　the observed $PM_{2.5}$, $O_3$, and $NO_2$ concentrations in the YRD region, especially in Shanghai. The daily concentrations of $PM_{2.5}$ are efficiently simulated in the five cities except Hefei, illustrated by the NMB, NME, and R values meeting the criteria established by Emery et al. (2017) (NMB ≤ ±0.30, NME ≤ 0.50, and R > 0.70). MDA8 $O_3$ are slightly overestimated in Nanjing, Hefei, Hangzhou, and Changzhou. Predicted

270　concentrations of $NO_2$ are generally lower than the observations in all five cities (–0.15 < NMB ≤ –0.05, –10.37 < MB ≤ –1.89). When compared to previous air quality simulation studies (Hu et al., 2016;Wang et al., 2021;Ma et al., 2021;Sulaymon et al., 2021;Li et al., 2021a), the results in this study show a better model performance.

Fig. 2 illustrates the comparison of predicted and observed $NO_3^-$ concentrations at

275　the four supersites on daily timescales (Fig. S2 shows the hourly predicted and observed $NO_3^-$ concentrations). The general temporal variations of observed $NO_3^-$ concentrations are efficiently captured by the model. Good agreement between predicted and observed values is demonstrated on daily timescales, especially in Shanghai (NMB = –0.49, R = 0.70), Hangzhou (NMB = 0.11, MB = 0.64) and Changzhou (NMB = 0.36, R = 0.56).

280　The seasonal daily concentrations of $NO_3^-$ are efficiently predicted in Shanghai, Hangzhou and Changzhou, within the benchmark (NMB ≤ ±0.60, NME ≤ 0.75, and R > 0.6). The performance statistical metrics of predicted $NO_3^-$ in this study are comparable to those of previous studies (Shi et al., 2017;Qu et al., 2021). $NO_3^-$ concentrations are generally underestimated during the summer and autumn. One possible reason is that

285　RH is slightly underestimated by the WRF model during these seasons (Table 1), which results in a lower buildup of $NO_3^-$ concentrations. Other reasons could be associated with uncertainties in the $NO_3^-$ formation mechanisms (i.e., missing or insufficient

heterogeneous reactions in the current CMAQ model) and uncertainties in NOx and NH$_3$ emissions (Zheng et al., 2020;Lu et al., 2021b;Zheng et al., 2015;Liu et al., 2019).

### 3.2. Regional transport contribution to nitrate in YRD

Fig. S3 shows the spatial distribution of the seasonal (winter, spring, summer and autumn) and annual mean (average of the four seasons) NO$_3^-$, HNO$_3$, and TNO$_3$ concentrations under four different emissions scenarios in the d02 domain. Under C$_{base}$, the seasonal and annual predicted concentrations of NO$_3^-$ for the entire YRD region were 16.0, 7.4, 1.0, 5.4, and 7.4 μg m$^{-3}$, respectively (Table S5). Compared to C$_{base}$, the seasonal and annual YRD NO$_3^-$ concentrations in C$_{outside-zero}$ decreased by 8.0, 2.8, 0.4, 2.2, and 3.3 μg m$^{-3}$, respectively. Even more significant differences in NO$_3^-$ are observed between C$_{base}$ and C$_{YRD-zero}$. The NO$_3^-$ values decreased by 12.0, 6.9, 0.9, 4.8 and 6.1 μg m$^{-3}$ in winter, spring, summer, autumn, and the year respectively, to become almost twice as high as those between C$_{base}$ and C$_{outside-zero}$. The results suggest that the YRD local anthropogenic emissions contribute more to the seasonal NO$_3^-$ concentrations.

Fig. 3 shows the regional contributions of the background, local, direct and indirect transport to nitrate-related species in the four seasons (results for Shanghai are shown in Fig S5). The local emissions dominate YRD NO$_3^-$, accounting for 50.4–62.0 % in the four seasons (Fig. 3a). Fig 3c suggests that the precursors (NO$_2$ and NH$_3$) are dominated by the local emissions (more than 93.0%). The contributions of the total regional transport (sum of indirect and direct transport) are 49.5, 38.0, 41.6, and 42.0 % in winter, spring, summer, and autumn, respectively. The indirect transport contributes 24.2–37.0% of NO$_3^-$ concentrations, and exceeds the contributions from direct transport in the spring, summer, and autumn. Similarly, Qu et al. (2021) reported that the reaction between the locally emitted NOx and transported O$_3$ dominates the production of indirect NO$_3^-$ transport in the PRD region.

In Fig. 3b, the local emission and indirect transport have negative contributions to O$_3$ concentration, leading to the depletion of O$_3$ in the four seasons. The local emissions

Atmospheric
Chemistry
and Physics
Discussions

Open Access

EGU

315    have negative contribution to $O_3$ in winter (–45.6%) and autumn (–12.3%), and the

indirect transport has negative contribution in spring (–8.5%) and autumn (–8.7%). For

$O_3$ and OH (Fig. 3b and 3d), indirect transport contributes about –8% and –12% – –42%

in all seasons, respectively. The negative contributions to $O_3$, $N_2O_5$, and OH suggest that

the atmospheric oxidants are consumed in YRD, which in turn enhances the chemical

320    production of $NO_3^-$.

### 3.3. Formation processes of nitrate

Fig. 4 shows the modeled diurnal variations of three nitrate-phases ($NO_3^-$, $HNO_3$,

and $TNO_3$), the major precursors (i.e., $O_3$, $NO_2$, and $NH_3$), and the major atmospheric

oxidants (OH and $N_2O_5$) in the four seasons for the entire YRD region in the base

325    scenario. Except for summer, higher predicted $TNO_3$ and $NO_3^-$ concentrations are

observed in early morning hours (6:00–8:00 am), while lower $TNO_3$ and $NO_3^-$

concentrations are observed around 16:00–18:00 pm. Predicted concentrations of $TNO_3$,

$HNO_3$, and $O_3$ show the same diurnal variations in the summer, and peak around 12:00

pm (the most active photochemical hours). The opposite profiles of $TNO_3$'s diurnal

330    variation between summer and non-summer are mainly attributed to the temperature

effect on the gas-to-particle partitioning between $NO_3^-$ and $HNO_3$. As shown in Fig. S3,

$NO_3^-$ dominates the $TNO_3$ concentrations and determines its diurnal variations in non-

summer, while $HNO_3$ dominates the diurnal variation in summer. A two-peak mode

diurnal variation of $NO_2$ and $NH_3$ is identified in the four seasons. High concentrations

335    of $NO_2$ and $NH_3$ occur in the early morning (hours 6:00–8:00 am) and early evening

(hours 18:00-19:00 pm), due to the local transportation emissions during rush hours.

OH and $N_2O_5$ have a one-peak mode diurnal variation in the four seasons. OH peaks

around 12:00 pm, similar to $HNO_3$, while $N_2O_5$ peaks around 18:00–20:00 pm.

Fig. S7 shows seasonal variations in $NO_3^-/PM_{2.5}$, $NO_3^-/TNO_3$, nitrogen oxidation

340    ratios (NOR = $[NO_3^-]/([NO_3^-] + [NO_2])$), and adjusted gas ratio (adjGR = $([NH_3] +$

$[NO_3^-])/([HNO_3] + [NO_3^-]))$ in YRD. $NO_3^-/PM_{2.5}$ and $NO_3^-/TNO_3$ are the highest in the

winter, accounting for 21 ± 5% and 94 ± 3%, respectively. The averaged NOR values for the entire YRD region are 0.24, 0.16, 0.03, and 0.13 mol/mol in winter, spring, summer, and autumn, respectively. The highest value of NOR in winter suggests a high

345    conversion efficiency of $NO_2$ to $NO_3^-$. AdjGR values are generally greater than two in the four seasons across most areas in YRD, indicating that YRD is mostly in the $NH_3$-rich regime. Therefore, $NH_3$ is not a limiting factor of $NO_3^-$ formation in YRD.

Fig. 5 illustrates a two-peak mode diurnal variation of the net IPRs rates of $NO_3^-$ production in the four seasons. Peak hours are around mid-noon (10:00–11:00 am) and

350    early evening (19:00–21:00 pm), with peak rates of 1.2–1.5, 0.7–0.8, 0.4–0.6, and 0.1–0.2 $\mu g\ m^{-3}\ h^{-1}$ in the winter, spring, summer, and autumn, respectively. AERO processes (including condensation, coagulation, and aerosol growth) are the dominant contributors of $NO_3^-$ formation, with the peak rates of 2.1, 1.3, 1.5, and 0.4 $\mu g\ m^{-3}\ h^{-1}$ in the winter, spring, summer, and autumn, respectively. The sharp decline hours of the

355    net IPRs (around 11:00–18:00 pm) are mainly dominated by TRAN (sum of HTRA and VTRA) processes, with the mean rates of –1.4, –0.8, –0.7, and –0.3 $\mu g\ m^{-3}\ h^{-1}$ in the winter, spring, summer, and autumn, respectively. However, in summer, TRAN processes constitute the dominant source during midnight (1:00–6:00 am), owing to higher $NO_3^-$ concentrations at the upper PBL contributing to the surface through the

360    vertical mixing and development of the PBL (Huang et al., 2020c). In Fig. S9, VTRA processes act as the main positive contributor to $NO_3^-$ buildup production from 0:00 to 23:00 at layer 1 (surface layer), while AERO processes make the negative contribution to $NO_3^-$ within layers 1–8 (from the surface to 800 m). Above layer 10, AERO processes for $NO_3^-$ production are positive in the daytime, which is conducive to the accumulation

365    of $NO_3^-$ concentrations.

For $HNO_3$, a one-peak mode diurnal variation of the net IPRs rates is found, and peak times are at 20:00 pm in the winter and around 9:00–12:00 am in other seasons (Fig. 5). Meanwhile, CHEM (gas chemical processes) processes are the major

contributor to $HNO_3$ formation, with the peak rates being 0.6, 1.4, 2.3, and 0.7 ppb h$^{-1}$

370 in the winter, spring, summer, and autumn, respectively. In the spring, summer and autumn, the peak times of $HNO_3$ formation are consistent with the first-peak times of $NO_3^-$. The seasonal net IPRs rates reached a maximum of 0.3, 1.0, and 0.1 ppb h$^{-1}$, respectively. CHEM and VTRA processes are the dominant contributors of $HNO_3^-$ production, especially during 7:00 to 13:00 (net IPRs rates > 0), with the seasonal peak

375 rates of 1.5, 2.7, and 0.8 ppb h$^{-1}$, respectively. AERO, DDEP, and HTRA processes are the dominant contributors of the $HNO_3^-$ sharp decline (14:00–17:00 pm), with the lowest net IPRs rates of –0.8, –0.7, and –0.3 μg m$^{-3}$ h$^{-1}$ in the spring, summer, and autumn, respectively. DDEP processes are the dominant sink of $HNO_3$ in summer (–0.64 ± 0.20 ppb h$^{-1}$). However, in the winter, the peak times of $HNO_3$ production are

380 opposite with the first-peak of $NO_3^-$, but consistent with the second-peak. HTRA make a positive contribution to $HNO_3^-$, with peak rates of 0.18 ppb h$^{-1}$ at 20:00 pm. In Fig. S12, the only-largest sink is the AERO process, consistent with efficient partitioning of $HNO_3$ into particle phase $NO_3^-$ in cold seasons.

Table 3 illustrates that within the PBL, in cold seasons (winter and autumn), about

385 60–78 % of $TNO_3$ is produced through OH+$NO_2$, 21–36 % through HET $N_2O_5$, and 2–5 % through the "Others" pathways in the five representative YRD cities. Meanwhile, 71–83 % of $TNO_3$ is produced through OH+$NO_2$, 10–23 % through HET $N_2O_5$, and 4–13 % through the "Others" pathways (mainly contributed by $NO_3$+Org and $N_2O_5$ $H_2O$) in warm seasons (summer and spring). Table 4 shows the comparison of the contribution

390 of the major $TNO_3$ production pathways studies in China and other regions using different methods. The results are in agreement with the contribution of $NO_3^-$ pathways in previous modeling and observational studies. For example, Li et al. (2021b) modeled that OH+$NO_2$ and HET $N_2O_5$ pathways dominate $NO_3^-$ production in the YRD region in warm and cold seasons of 2016 by the CTM, accounting for 86–92 % and 8–14 % in

395 the surface layer, respectively. He et al. (2020) reported that the OH+$NO_2$ pathway

dominates $NO_3^-$ production in Shanghai on the surface layer using nitrogen isotopes analysis, accounting for 84–92 % and 55–77 % in the warm and cold seasons of 2016, respectively. Alexander et al. (2020) highlighted that the $OH+NO_2$ and HET $N_2O_5$ pathways contribute the same proportion (both 41 % in the four seasons) to $NO_3^-$ production in the global region using the CTM and oxygen isotopes analysis.

Fig. 6a shows the diurnal variations of $TNO_3$ formation reactions rates through three major pathways in Shanghai within the PBL. The average diurnal trends of $TNO_3$ production rates are consistent with the CHEM processes rates of $HNO_3$ production (Figs. 5–6). The chemical production of $HNO_3$ quickly transforms to particulate $NO_3^-$, through AERO processes in the presence of abundant $NH_3$. In the winter, spring, summer, and autumn, the averaged $TNO_3$ production rates are $0.31 \pm 0.14$, $0.65 \pm 0.37$, $1.09 \pm 0.68$, and $0.28 \pm 0.22$ ppb h$^{-1}$, respectively (Table S6). Moreover, the seasonal peak rates of $TNO_3$ production are 0.6, 1.4, 2.3, and 0.7 ppb h$^{-1}$ around 11:00 am –13:00 pm, respectively. In accordance with the seasonal variation of $HNO_3$ net IPRs rates, $TNO_3$ production rates are the fastest in summer.

In Shanghai, $TNO_3$ chemical production is dominated by the $OH+NO_2$ pathway on the daily timescale, accounting for 69.3–86.9 % of the total, while the HET $N_2O_5$ pathway is likewise a relatively important pathway (accounting for 11.1–28.4 %) in the four seasons (Fig. 6b). Notably, $TNO_3$ production rates are dominated by the $OH+NO_2$ pathway during the daytime (7:00 am–18:00 pm, accounting for 88.4–97.9 % of the total) in all seasons, while the HET $N_2O_5$ pathway becomes more important for the $TNO_3$ production during the nighttime (19:00 pm – 06:00 am, accounting for 42.5–61.6%). During winter, $TNO_3$ formation via the HET $N_2O_5$ pathway becomes dominant over the $OH+NO_2$ pathway, accounting for 62, 65, and 68% in Shanghai, Hangzhou and Nanjing at night, respectively. $O_3$ strongly coordinates $TNO_3$ production in YRD via the HET $N_2O_5$ pathway during the nighttime. Similarly, He et al. (2018) observed that the HET $N_2O_5$ pathway was the major contributor to $NO_3^-$ production in the winter

of Beijing at the surface layer, using oxygen and nitrogen isotopes analysis, accounting for 56–97 % of the total during the nighttime. In another CTM study in the NCP, the

425    HET $N_2O_5$ pathway was the dominant contributor to nocturnal-$NO_3^-$ production within the PBL in winter, with a contribution of 83 % at night (Liu et al., 2020a).

Fig. 7 displays the contributions of $TNO_3$ formation pathways from the local and transport (sum of indirect and direct transport) contributions. For the local contribution, the averaged $TNO_3$ production rates are $0.27 \pm 0.14$, $0.56 \pm 0.37$, $1.05 \pm 0.69$, and 0.26

430    $\pm 0.21$ ppb $h^{-1}$ in the winter, spring, summer, and autumn, respectively (Table S8). During the daytime, the $OH+NO_2$ pathway contributes almost all $TNO_3$ production rates from the local contribution, accounting for about 89–98 % of the total, with mean rates of $0.33 \pm 0.17$, $0.83 \pm 0.34$, $1.55 \pm 0.59$, and $0.40 \pm 0.22$ ppb $h^{-1}$ in the winter, spring, summer, and autumn, respectively. The results suggest that the locally-emitted

435    $NO_2$ reacts with locally-formed OH dominated $TNO_3$ production rates during the day in the urban YRD region. For the transport contribution, the averaged $TNO_3$ production rates are $0.04 \pm 0.01$, $0.08 \pm 0.02$, $0.03 \pm 0.02$, and $0.02 \pm 0.01$ ppb $h^{-1}$ in the winter, spring, summer, and autumn, respectively (Table S9). The HET $N_2O_5$ pathway is noted as the dominant pathway for $TNO_3$ production of the transport contribution, accounting

440    for around 72–86 % during the nighttime. Fig. 7b compares the $TNO_3$ production pathways rates between indirect and direct transport contributions. The regional production is mainly contributed by indirect transport, especially in the winter and summer. The results suggest that the transported $O_3$ from outside YRD region can react with the locally-emitted $NO_2$, supporting $HNO_3$ formation production via the HET $N_2O_5$

445    chemistry pathway at night.

## *4. Conclusions*

This study investigates the contributions of regional transport and major chemical pathways to the of $NO_3^-$ and $HNO_3$ formation in YRD in different seasons using the

450 WRF-CMAQ model. The modeled results show that local emissions dominate YRD-regional $NO_3^-$ concentrations (50–62%), while regional transport contributes 38–50% to $NO_3^-$ (indirect transport contributes 24–37%). Except for winter, $HNO_3$ was dominated by the contributions of local emissions (61–75%) and indirect transport contributed negatively –24 to –41%. In Shanghai, the IPRs analysis reveals that AERO processes were the predominant contributors in $NO_3^-$ formation within the PBL. TRAN

455 processes were the largest sinks in $NO_3^-$ formation in the winter, spring and autumn, while the positive contributors at night in summer. For $HNO_3$, CHEM processes were the only positive contributor during the day. The $OH+NO_2$ pathway is the predominant contributor (60–83%) among all chemical pathways, while the HET $N_2O_5$ pathway is also important (10–36%) in YRD. The $TNO_3$ production is dominated by the $OH+NO_2$

460 pathway during the day (98%) in summer, while the HET $N_2O_5$ pathway dominates during the night (61%) in winter. The $TNO_3$ production rates from the local and transport contributions were further elucidated. The $OH+NO_2$ pathway from the local contribution strongly dominates the $TNO_3$ production during the day (89–98%). At night, the HET $N_2O_5$ pathway mainly dominate by indirect transport (via reaction with

465 transported $O_3$ at night).

### Code and data availability

Hourly concentrations of $O_3$, $PM_{2.5}$, $NO_2$, $SO_2$, and CO used in this study are freely available through the website of http://106.37.208.233:20035/ (last accessed on April

470 30, 2022). Observation data of meteorological parameters used in this study are available from http://data.cma.cn/en (last accessed on November 30, 2021). The CMAQ outputs are currently available upon request, all python codes used to create any of the figures are available upon request.

Atmospheric
Chemistry
and Physics

Discussions

## Author contributions

475

JS, MQ and JH designed research. JS, MQ, XX, WF, YQ, LS, and LL contributed to model development, simulations, and data processing. JL, IS, LJ, LH, XY contributed to result discussion. JS prepared the manuscript and all coauthors helped improve the manuscript.

480

## Competing interests

The authors declare that they have no conflict of interest.

## Acknowledgements

## References

Alexander, B., Sherwen, T., Holmes, C. D., Fisher, J. A., Chen, Q., Evans, M. J., and Kasibhatla, P.:
490 Global inorganic nitrate production mechanisms: comparison of a global model with nitrate isotope observations, Atmos. Chem. Phys., 20, 3859-3877, 10.5194/acp-20-3859-2020, 2020.
An, J., Huang, Y., Huang, C., Wang, X., Yan, R., Wang, Q., Wang, H., Jing, S., Zhang, Y., Liu, Y., Chen, Y., Xu, C., Qiao, L., Zhou, M., Zhu, S., Hu, Q., Lu, J., and Chen, C.: Emission inventory of air pollutants and chemical speciation for specific anthropogenic sources based on local measurements in the Yangtze
495 River Delta region, China, Atmos. Chem. Phys., 21, 2003-2025, 10.5194/acp-21-2003-2021, 2021.
Byun, D., and Schere, K. L.: Review of the Governing Equations, Computational Algorithms, and Other Components of the Models-3 Community Multiscale Air Quality (CMAQ) Modeling System, ApMRv, 59, 51-77, 10.1115/1.2128636, 2006.
Chan, Y.-C., Evans, M. J., He, P., Holmes, C. D., Jaeglé, L., Kasibhatla, P., Liu, X.-Y., Sherwen, T.,
500 Thornton, J. A., Wang, X., Xie, Z., Zhai, S., and Alexander, B.: Heterogeneous Nitrate Production Mechanisms in Intense Haze Events in the North China Plain, Journal of Geophysical Research:

Atmospheres, 126, e2021JD034688, https://doi.org/10.1029/2021JD034688, 2021.

Chen, T.-F., Chang, K.-H., and Lee, C.-H.: Simulation and analysis of causes of a haze episode by combining CMAQ-IPR and brute force source sensitivity method, Atmos. Environ., 218, 117006, https://doi.org/10.1016/j.atmosenv.2019.117006, 2019.

Chen, X., Jiang, Z., Shen, Y., Li, R., Fu, Y., Liu, J., Han, H., Liao, H., Cheng, X., Jones, D. B. A., Worden, H., and Abad, G. G.: Chinese Regulations Are Working—Why Is Surface Ozone Over Industrialized Areas Still High? Applying Lessons From Northeast US Air Quality Evolution, Geophys. Res. Lett., 48, e2021GL092816, https://doi.org/10.1029/2021GL092816, 2021.

Chen, X. R., Wang, H. C., Lu, K. D., Li, C., Zhai, T., Tan, Z., Ma, X., Yang, X., Liu, Y., Chen, S., Dong, H., Li, X., Wu, Z., Hu, M., Zeng, L., and Zhang, Y.: Field Determination of Nitrate Formation Pathway in Winter Beijing, Environ. Sci. Technol., 54, 9243-9253, 10.1021/acs.est.0c00972, 2020.

Chuang, M.-T., Wu, C.-F., Lin, C.-Y., Lin, W.-C., Chou, C. C. K., Lee, C.-T., Lin, T.-H., Fu, J. S., and Kong, S. S.-K.: Simulating nitrate formation mechanisms during PM2.5 events in Taiwan and their implications for the controlling direction, Atmos. Environ., 269, 118856, https://doi.org/10.1016/j.atmosenv.2021.118856, 2022.

Dai, H. B., Zhu, J., Liao, H., Li, J., Liang, M., Yang, Y., and Yue, X.: Co-occurrence of ozone and PM2.5 pollution in the Yangtze River Delta over 2013–2019: Spatiotemporal distribution and meteorological conditions, Atmos. Res., 249, 105363, https://doi.org/10.1016/j.atmosres.2020.105363, 2021.

Ding, A. J., Huang, X., Nie, W., Chi, X., Xu, Z., Zheng, L., Xu, Z., Xie, Y., Qi, X., Shen, Y., Sun, P., Wang, J., Wang, L., Sun, J., Yang, X. Q., Qin, W., Zhang, X., Cheng, W., Liu, W., Pan, L., and Fu, C.: Significant reduction of PM2.5 in eastern China due to regional-scale emission control: evidence from SORPES in 2011–2018, Atmos. Chem. Phys., 19, 11791-11801, 10.5194/acp-19-11791-2019, 2019.

Du, H., Li, J., Wang, Z., Dao, X., Guo, S., Wang, L., Ma, S., Wu, J., Yang, W., Chen, X., and Sun, Y.: Effects of Regional Transport on Haze in the North China Plain: Transport of Precursors or Secondary Inorganic Aerosols, Geophys. Res. Lett., 47, e2020GL087461, 10.1029/2020gl087461, 2020.

Emery, C., and Tai, E.: Enhanced Meteorological Modeling and Performance Evaluation for Two Texas Ozone Episodes, Final Report Submitted to Texas Natural Resources Conservation Commission, 2001.

Emery, C., Liu, Z., Russell, A. G., Odman, M. T., Yarwood, G., and Kumar, N.: Recommendations on statistics and benchmarks to assess photochemical model performance, J. Air Waste Manage. Assoc., 67, 582-598, 10.1080/10962247.2016.1265027, 2017.

Fan, M.-Y., Zhang, Y.-L., Lin, Y.-C., Cao, F., Zhao, Z.-Y., Sun, Y., Qiu, Y., Fu, P., and Wang, Y.: Changes of Emission Sources to Nitrate Aerosols in Beijing After the Clean Air Actions: Evidence From Dual Isotope Compositions, Journal of Geophysical Research: Atmospheres, 125, e2019JD031998, 10.1029/2019JD031998, 2020.

Fan, M.-Y., Zhang, Y.-L., Lin, Y.-C., Hong, Y., Zhao, Z.-Y., Xie, F., Du, W., Cao, F., Sun, Y., and Fu, P.: Important Role of NO3 Radical to Nitrate Formation Aloft in Urban Beijing: Insights from Triple Oxygen Isotopes Measured at the Tower, Environ. Sci. Technol., 10.1021/acs.est.1c02843, 2021.

Fu, X., Wang, T., Gao, J., Wang, P., Liu, Y., Wang, S., Zhao, B., and Xue, L.: Persistent Heavy Winter Nitrate Pollution Driven by Increased Photochemical Oxidants in Northern China, Environ. Sci. Technol., 54, 3881-3889, 10.1021/acs.est.9b07248, 2020.

Griffith, S. M., Huang, X. H. H., Louie, P. K. K., and Yu, J. Z.: Characterizing the thermodynamic and chemical composition factors controlling PM2.5 nitrate: Insights gained from two years of online measurements in Hong Kong, Atmos. Environ., 122, 864-875, https://doi.org/10.1016/j.atmosenv.2015.02.009, 2015.

Guenther, A. B., Jiang, X., Heald, C. L., Sakulyanontvittaya, T., Duhl, T., Emmons, L. K., and Wang, X.: The Model of Emissions of Gases and Aerosols from Nature version 2.1 (MEGAN2.1): an extended and updated framework for modeling biogenic emissions, Geosci. Model Dev., 5, 1471-1492, 10.5194/gmd-5-1471-2012, 2012.

550    Guo, H., Otjes, R., Schlag, P., Kiendler-Scharr, A., Nenes, A., and Weber, R. J.: Effectiveness of ammonia reduction on control of fine particle nitrate, Atmos. Chem. Phys., 18, 12241-12256, 10.5194/acp-18-12241-2018, 2018.

He, P., Xie, Z., Chi, X., Yu, X., Fan, S., Kang, H., Liu, C., and Zhan, H.: Atmospheric Δ17O(NO3−) reveals nocturnal chemistry dominates nitrate production in Beijing haze, Atmos. Chem. Phys., 18,

555    14465-14476, 10.5194/acp-18-14465-2018, 2018.

He, P., Xie, Z., Yu, X., Wang, L., Kang, H., and Yue, F.: The observation of isotopic compositions of atmospheric nitrate in Shanghai China and its implication for reactive nitrogen chemistry, Sci. Total Environ., 714, 136727, https://doi.org/10.1016/j.scitotenv.2020.136727, 2020.

Hu, J., Chen, J., Ying, Q., and Zhang, H.: One-year simulation of ozone and particulate matter in China

560    using WRF/CMAQ modeling system, Atmos. Chem. Phys., 16, 10333-10350, 10.5194/acp-16-10333-2016, 2016.

Hu, S., Zhao, G., Tan, T., Li, C., Zong, T., Xu, N., Zhu, W., and Hu, M.: Current challenges of improving visibility due to increasing nitrate fraction in PM2.5 during the haze days in Beijing, China, Environ. Pollut., 290, 118032, https://doi.org/10.1016/j.envpol.2021.118032, 2021.

565    Huang, L., Zhu, Y., Zhai, H., Xue, S., Zhu, T., Shao, Y., Liu, Z., Emery, C., Yarwood, G., Wang, Y., Fu, J., Zhang, K., and Li, L.: Recommendations on benchmarks for numerical air quality model applications in China – Part 1: PM2.5 and chemical species, Atmos. Chem. Phys., 21, 2725-2743, 10.5194/acp-21-2725-2021, 2021.

Huang, R. J., Zhang, Y. L., Bozzetti, C., Ho, K.-F., Cao, J.-J., Han, Y., Daellenbach, K. R., Slowik, J. G.,

570    Platt, S. M., Canonaco, F., Zotter, P., Wolf, R., Pieber, S. M., Bruns, E. A., Crippa, M., Ciarelli, G., Piazzalunga, A., Schwikowski, M., Abbaszade, G., Schnelle-Kreis, J., Zimmermann, R., An, Z., Szidat, S., Baltensperger, U., Haddad, I. E., and Prévôt, A. S. H.: High secondary aerosol contribution to particulate pollution during haze events in China, Nature, 514, 218-222, 10.1038/nature13774, 2014.

Huang, X., Ding, A., Wang, Z., Ding, K., Gao, J., Chai, F., and Fu, C.: Amplified transboundary transport

575    of haze by aerosol–boundary layer interaction in China, Nat. Geosci., 13, 428-434, 10.1038/s41561-020-0583-4, 2020a.

Huang, X., Ding, A. J., Gao, J., Zheng, B., Zhou, D., Qi, X., Tang, R., Wang, J., Ren, C., Nie, W., Chi, X., Xu, Z., Chen, L., Li, Y., Che, F., Pang, N., Wang, H., Tong, D., Qin, W., Cheng, W., Liu, W., Fu, Q., Liu, B., Chai, F., Davis, S. J., Zhang, Q., and He, K.: Enhanced secondary pollution offset reduction of

580    primary emissions during COVID-19 lockdown in China, Natl. Sci. Rev., 8, nwaa137, 10.1093/nsr/nwaa137, 2020b.

Huang, X., Huang, J. T., Ren, C. H., Wang, J., Wang, H., Wang, J., Yu, H., Chen, J., Gao, J., and Ding, A.: Chemical Boundary Layer and Its Impact on Air Pollution in Northern China, Environ. Sci. Technol. Lett., 10.1021/acs.estlett.0c00755, 2020c.

585    Itahashi, S., Uno, I., Osada, K., Kamiguchi, Y., Yamamoto, S., Tamura, K., Wang, Z., Kurosaki, Y., and Kanaya, Y.: Nitrate transboundary heavy pollution over East Asia in winter, Atmos. Chem. Phys., 17, 3823-3843, 10.5194/acp-17-3823-2017, 2017.

Khezri, B., Mo, H., Yan, Z., Chong, S.-L., Heng, A. K., and Webster, R. D.: Simultaneous online monitoring of inorganic compounds in aerosols and gases in an industrialized area, Atmos. Environ., 80,

590    352-360, https://doi.org/10.1016/j.atmosenv.2013.08.008, 2013.

Kim, Y. J., Spak, S. N., Carmichael, G. R., Riemer, N., and Stanier, C. O.: Modeled aerosol nitrate formation pathways during wintertime in the Great Lakes region of North America, Journal of Geophysical Research: Atmospheres, 119, 12,420-412,445, https://doi.org/10.1002/2014JD022320, 2014.

595    Li, C., Hammer, M. S., Zheng, B., and Cohen, R. C.: Accelerated reduction of air pollutants in China, 2017-2020, Sci. Total Environ., 803, 150011, https://doi.org/10.1016/j.scitotenv.2021.150011, 2022.

Li, L., Xie, F., Li, J., Gong, K., Xie, X., Qin, Y., Qin, M., and Hu, J.: Diagnostic analysis of regional ozone pollution in Yangtze River Delta, China: A case study in summer 2020, Sci. Total Environ., 151511, https://doi.org/10.1016/j.scitotenv.2021.151511, 2021a.

600    Li, M., Zhang, Z., Yao, Q., Wang, T., Xie, M., Li, S., Zhuang, B., and Han, Y.: Nonlinear responses of particulate nitrate to NOx emission controls in the megalopolises of China, Atmos. Chem. Phys., 21, 15135-15152, 10.5194/acp-21-15135-2021, 2021b.

Lin, Y. C., Zhang, Y. L., Fan, M. Y., and Bao, M.: Heterogeneous formation of particulate nitrate under ammonium-rich regimes during the high-PM2.5 events in Nanjing, China, Atmos. Chem. Phys., 20,
605    3999-4011, 10.5194/acp-20-3999-2020, 2020.

Liu, L., Liu, L., Liu, S., Li, X., Zhou, J., Feng, T., Cao, J., Qian, Y., Cao, J., and Li, G.: Effects of organic coating on the nitrate formation by suppressing the N2O5 heterogeneous hydrolysis: A case study during wintertime in Beijing-Tianjin-Hebei (BTH), Atmos. Chem. Phys., 19, 8189-8207, 10.5194/acp-19-8189-2019, 2019.

610    Liu, L., Bei, N., Hu, B., Wu, J., Liu, S., Li, X., Wang, R., Liu, Z., Shen, Z., and Li, G.: Wintertime nitrate formation pathways in the north China plain: Importance of N2O5 heterogeneous hydrolysis, Environ. Pollut., 266, 115287, https://doi.org/10.1016/j.envpol.2020.115287, 2020a.

Liu, P., Zhang, Y., Yu, S., and Schere, K. L.: Use of a process analysis tool for diagnostic study on fine particulate matter predictions in the U.S.–Part II: Analyses and sensitivity simulations, Atmospheric
615    Pollution Research, 2, 61-71, https://doi.org/10.5094/APR.2011.008, 2011.

Liu, T., Wang, X. Y., Hu, J. L., Wang, Q., An, J., Gong, K., Sun, J., Li, L., Qin, M., Li, J., Tian, J., Huang, Y., Liao, H., Zhou, M., Hu, Q., Yan, R., Wang, H., and Huang, C.: Driving Forces of Changes in Air Quality during the COVID-19 Lockdown Period in the Yangtze River Delta Region, China, Environ. Sci. Technol. Lett., 7, 779-786, 10.1021/acs.estlett.0c00511, 2020b.

620    Lu, M., Tang, X., Feng, Y., Wang, Z., Chen, X., Kong, L., Ji, D., Liu, Z., Liu, K., Wu, H., Liang, S., Zhou, H., and Hu, K.: Nonlinear response of SIA to emission changes and chemical processes over eastern and central China during a heavy haze month, Sci. Total Environ., 788, 147747, https://doi.org/10.1016/j.scitotenv.2021.147747, 2021a.

Lu, X., Ye, X., Zhou, M., Zhao, Y., Weng, H., Kong, H., Li, K., Gao, M., Zheng, B., Lin, J., Zhou, F.,
625    Zhang, Q., Wu, D., Zhang, L., and Zhang, Y.: The underappreciated role of agricultural soil nitrogen oxide emissions in ozone pollution regulation in North China, Nature Communications, 12, 5021, 10.1038/s41467-021-25147-9, 2021b.

Luo, L., Kao, S., Wu, Y., Zhang, X., Lin, H., Zhang, R., and Xiao, H.: Stable oxygen isotope constraints on nitrate formation in Beijing in springtime, Environ. Pollut., 263, 114515,
630    https://doi.org/10.1016/j.envpol.2020.114515, 2020a.

Luo, L., Pan, Y.-Y., Zhu, R.-G., Zhang, Z.-Y., Zheng, N.-J., Liu, Y.-H., Liu, C., Xiao, H.-W., and Xiao, H.-Y.: Assessment of the seasonal cycle of nitrate in PM2.5 using chemical compositions and stable nitrogen and oxygen isotopes at Nanchang, China, Atmos. Environ., 225, 117371,

22

Atmospheric
Chemistry
and Physics
Discussions

https://doi.org/10.1016/j.atmosenv.2020.117371, 2020b.

635   Ma, J., Shen, J., Wang, P., Zhu, S., Wang, Y., Wang, P., Wang, G., Chen, J., and Zhang, H.: Modeled changes in source contributions of particulate matter during the COVID-19 pandemic in the Yangtze River Delta, China, Atmos. Chem. Phys., 21, 7343-7355, 10.5194/acp-21-7343-2021, 2021.

Prabhakar, G., Parworth, C. L., Zhang, X., Kim, H., Young, D. E., Beyersdorf, A. J., Ziemba, L. D., Nowak, J. B., Bertram, T. H., Faloona, I. C., Zhang, Q., and Cappa, C. D.: Observational assessment of

640   the role of nocturnal residual-layer chemistry in determining daytime surface particulate nitrate concentrations, Atmos. Chem. Phys., 17, 14747-14770, 10.5194/acp-17-14747-2017, 2017.

Qiao, X., Tang, Y., Hu, J., Zhang, S., Li, J., Kota, S. H., Wu, L., Gao, H., Zhang, H., and Ying, Q.: Modeling dry and wet deposition of sulfate, nitrate, and ammonium ions in Jiuzhaigou National Nature Reserve, China using a source-oriented CMAQ model: Part I. Base case model results, Sci. Total Environ.,

645   532, 831-839, https://doi.org/10.1016/j.scitotenv.2015.05.108, 2015.

Qin, Y., Li, J. Y., Gong, K. J., Wu, Z., Chen, M., Qin, M., Huang, L., and Hu, J.: Double high pollution events in the Yangtze River Delta from 2015 to 2019: Characteristics, trends, and meteorological situations, Sci. Total Environ., 792, 148349, https://doi.org/10.1016/j.scitotenv.2021.148349, 2021.

Qu, K., Wang, X. S., Xiao, T., Shen, J., Lin, T., Chen, D., He, L.-Y., Huang, X.-F., Zeng, L., Lu, K., Ou,

650   Y., and Zhang, Y.: Cross-regional transport of PM2.5 nitrate in the Pearl River Delta, China: Contributions and mechanisms, Sci. Total Environ., 753, 142439, https://doi.org/10.1016/j.scitotenv.2020.142439, 2021.

Shah, V., Jaeglé, L., Thornton, J. A., Lopez-Hilfiker, F. D., Lee, B. H., Schroder, J. C., Campuzano-Jost, P., Jimenez, J. L., Guo, H., Sullivan, A. P., Weber, R. J., Green, J. R., Fiddler, M. N., Bililign, S., Campos,

655   T. L., Stell, M., Weinheimer, A. J., Montzka, D. D., and Brown, S. S.: Chemical feedbacks weaken the wintertime response of particulate sulfate and nitrate to emissions reductions over the eastern United States, Proceedings of the National Academy of Sciences, 115, 8110-8115, 10.1073/pnas.1803295115, 2018.

Shen, J. Y., Zhao, Q. B., Cheng, Z., Wang, P., Ying, Q., Liu, J., Duan, Y., and Fu, Q.: Insights into source

660   origins and formation mechanisms of nitrate during winter haze episodes in the Yangtze River Delta, Sci. Total Environ., 741, 140187, https://doi.org/10.1016/j.scitotenv.2020.140187, 2020.

Sheng, L., Qin, M., Li, L., Wang, C., Gong, K., Liu, T., Li, J., and Hu, J.: Impacts of emissions along the lower Yangtze River on air quality and public health in the Yangtze River delta, China, Atmospheric Pollution Research, 101420, https://doi.org/10.1016/j.apr.2022.101420, 2022.

665   Shi, Z., Li, J., Huang, L., Wang, P., Wu, L., Ying, Q., Zhang, H., Lu, L., Liu, X., Liao, H., and Hu, J.: Source apportionment of fine particulate matter in China in 2013 using a source-oriented chemical transport model, Sci. Total Environ., 601-602, 1476-1487, https://doi.org/10.1016/j.scitotenv.2017.06.019, 2017.

Sulaymon, I. D., Zhang, Y., Hu, J., Hopke, P. K., Zhang, Y., Zhao, B., Xing, J., Li, L., and Mei, X.:

670   Evaluation of regional transport of PM2.5 during severe atmospheric pollution episodes in the western Yangtze River Delta, China, J. Environ. Manage., 293, 112827, https://doi.org/10.1016/j.jenvman.2021.112827, 2021.

Sun, J. J., Liang, M. J., Shi, Z. H., Shen, F., Li, J., Huang, L., Ge, X., Chen, Q., Sun, Y., Zhang, Y., Chang, Y., Ji, D., Ying, Q., Zhang, H., Kota, S. H., and Hu, J.: Investigating the PM2.5 mass concentration growth

675   processes during 2013–2016 in Beijing and Shanghai, Chemosphere, 221, 452-463, https://doi.org/10.1016/j.chemosphere.2018.12.200, 2019.

Tan, Z. F., Wang, H. C., Lu, K. D., Dong, H. B., Liu, Y. H., Zeng, L. M., Hu, M., and Zhang, Y. H.: An

Observational Based Modeling of the Surface Layer Particulate Nitrate in the North China Plain During Summertime, J Geophys Res-Atmos, 126, e2021JD035623, ARTN e2021JD035623

680  10.1029/2021JD035623, 2021.

Vrekoussis, M., Kanakidou, M., Mihalopoulos, N., Crutzen, P. J., Lelieveld, J., Perner, D., Berresheim, H., and Baboukas, E.: Role of the $NO_3$ radicals in oxidation processes in the eastern Mediterranean troposphere during the MINOS campaign, Atmos. Chem. Phys., 4, 169-182, 10.5194/acp-4-169-2004, 2004.

685  Wang, H., Lu, K., Chen, X., Zhu, Q., Wu, Z., Wu, Y., and Sun, K.: Fast particulate nitrate formation via N2O5 uptake aloft in winter in Beijing, Atmos. Chem. Phys., 18, 10483-10495, 10.5194/acp-18-10483-2018, 2018.

Wang, J., Gao, J., Che, F., Wang, Y., Lin, P., and Zhang, Y.: Decade-long trends in chemical component properties of PM2.5 in Beijing, China (2011−2020), Sci. Total Environ., 154664,

690  https://doi.org/10.1016/j.scitotenv.2022.154664, 2022.

Wang, X., Li, L., Gong, K., Mao, J., Hu, J., Li, J., Liu, Z., Liao, H., Qiu, W., Yu, Y., Dong, H., Guo, S., Hu, M., Zeng, L., and Zhang, Y.: Modelling air quality during the EXPLORE-YRD campaign – Part I. Model performance evaluation and impacts of meteorological inputs and grid resolutions, Atmos. Environ., 246, 118131, https://doi.org/10.1016/j.atmosenv.2020.118131, 2021.

695  Wang, Y.-L., Song, W., Yang, W., Sun, X.-C., Tong, Y.-D., Wang, X.-M., Liu, C.-Q., Bai, Z.-P., and Liu, X.-Y.: Influences of Atmospheric Pollution on the Contributions of Major Oxidation Pathways to PM2.5 Nitrate Formation in Beijing, Journal of Geophysical Research: Atmospheres, 124, 4174-4185, https://doi.org/10.1029/2019JD030284, 2019.

Wen, L., Xue, L., Wang, X., Xu, C., Chen, T., Yang, L., Wang, T., Zhang, Q., and Wang, W.: Summertime

700  fine particulate nitrate pollution in the North China Plain: increasing trends, formation mechanisms and implications for control policy, Atmos. Chem. Phys., 18, 11261-11275, 10.5194/acp-18-11261-2018, 2018.

Wiedinmyer, C., Akagi, S. K., Yokelson, R. J., Emmons, L. K., Al-Saadi, J. A., Orlando, J. J., and Soja, A. J.: The Fire INventory from NCAR (FINN): a high resolution global model to estimate the emissions

705  from open burning, Geosci. Model Dev., 4, 625-641, 10.5194/gmd-4-625-2011, 2011.

Womack, C. C., McDuffie, E. E., Edwards, P. M., Bares, R., de Gouw, J. A., Docherty, K. S., Dubé, W. P., Fibiger, D. L., Franchin, A., Gilman, J. B., Goldberger, L., Lee, B. H., Lin, J. C., Long, R., Middlebrook, A. M., Millet, D. B., Moravek, A., Murphy, J. G., Quinn, P. K., Riedel, T. P., Roberts, J. M., Thornton, J. A., Valin, L. C., Veres, P. R., Whitehill, A. R., Wild, R. J., Warneke, C., Yuan, B.,

710  Baasandorj, M., and Brown, S. S.: An Odd Oxygen Framework for Wintertime Ammonium Nitrate Aerosol Pollution in Urban Areas: NOx and VOC Control as Mitigation Strategies, Geophys. Res. Lett., 46, 4971-4979, https://doi.org/10.1029/2019GL082028, 2019.

Wu, C., Liu, L., Wang, G., Zhang, S., Li, G., Lv, S., Li, J., Wang, F., Meng, J., and Zeng, Y.: Important contribution of N2O5 hydrolysis to the daytime nitrate in Xi'an, China during haze periods: Isotopic

715  analysis and WRF-Chem model simulation, Environ. Pollut., 288, 117712, https://doi.org/10.1016/j.envpol.2021.117712, 2021.

Wu, J.-B., Wang, Z., Wang, Q., Li, J., Xu, J., Chen, H., Ge, B., Zhou, G., and Chang, L.: Development of an on-line source-tagged model for sulfate, nitrate and ammonium: A modeling study for highly polluted periods in Shanghai, China, Environ. Pollut., 221, 168-179,

720  https://doi.org/10.1016/j.envpol.2016.11.061, 2017.

Wyat Appel, K., Napelenok, S., Hogrefe, C., Pouliot, G., Foley, K. M., Roselle, S. J., Pleim, J. E., Bash,

J., Pye, H. O. T., Heath, N., Murphy, B., and Mathur, R.: Overview and Evaluation of the Community Multiscale Air Quality (CMAQ) Modeling System Version 5.2, Air Pollution Modeling and its Application XXV, Cham, 2018, 69-73.

725    Xie, Y., Wang, G., Wang, X., Chen, J., Chen, Y., Tang, G., Wang, L., Ge, S., Xue, G., Wang, Y., and Gao, J.: Nitrate-dominated PM2.5 and elevation of particle pH observed in urban Beijing during the winter of 2017, Atmos. Chem. Phys., 20, 5019-5033, 10.5194/acp-20-5019-2020, 2020.

Yang, X., Wu, K., Wang, H., Liu, Y., Gu, S., Lu, Y., Zhang, X., Hu, Y., Ou, Y., Wang, S., and Wang, Z.: Summertime ozone pollution in Sichuan Basin, China: Meteorological conditions, sources and process

730    analysis, Atmos. Environ., 226, 117392, https://doi.org/10.1016/j.atmosenv.2020.117392, 2020.

Ying, Q., Wu, L., and Zhang, H.: Local and inter-regional contributions to PM2.5 nitrate and sulfate in China, Atmos. Environ., 94, 582-592, https://doi.org/10.1016/j.atmosenv.2014.05.078, 2014.

Zang, H., Zhao, Y., Huo, J., Zhao, Q., Fu, Q., Duan, Y., Shao, J., Huang, C., An, J., Xue, L., Li, Z., Li, C., and Xiao, H.: High atmospheric oxidation capacity drives wintertime nitrate pollution in the eastern

735    Yangtze River Delta of China, Atmos. Chem. Phys., 22, 4355-4374, 10.5194/acp-22-4355-2022, 2022.

Zhai, S. X., Jacob, D. J., Wang, X., Liu, Z., Wen, T., Shah, V., Li, K., Moch, J. M., Bates, K. H., Song, S., Shen, L., Zhang, Y., Luo, G., Yu, F., Sun, Y., Wang, L., Qi, M., Tao, J., Gui, K., Xu, H., Zhang, Q., Zhao, T., Wang, Y., Lee, H. C., Choi, H., and Liao, H.: Control of particulate nitrate air pollution in China, Nat. Geosci., 14, 389-395, 10.1038/s41561-021-00726-z, 2021.

740    Zhang, Z., Cao, L., Liang, Y., Guo, W., Guan, H., and Zheng, N.: Importance of NO3 radical in particulate nitrate formation in a southeast Chinese urban city: New constraints by δ15N-δ18O space of NO3, Atmos. Environ., 253, 118387, https://doi.org/10.1016/j.atmosenv.2021.118387, 2021.

Zheng, B., Zhang, Q., Zhang, Y., He, K. B., Wang, K., Zheng, G. J., Duan, F. K., Ma, Y. L., and Kimoto, T.: Heterogeneous chemistry: A mechanism missing in current models to explain secondary inorganic

745    aerosol formation during the January 2013 haze episode in North China, Atmos. Chem. Phys., 15, 2031-2049, 10.5194/acp-15-2031-2015, 2015.

Zheng, B., Tong, D., Li, M., Liu, F., Hong, C., Geng, G., Li, H., Li, X., Peng, L., Qi, J., Yan, L., Zhang, Y., Zhao, H., Zheng, Y., He, K., and Zhang, Q.: Trends in China's anthropogenic emissions since 2010 as the consequence of clean air actions, Atmos. Chem. Phys., 18, 14095-14111, 10.5194/acp-18-14095-

750    2018, 2018.

Zheng, H., Song, S., Sarwar, G., Gen, M., Wang, S., Ding, D., Chang, X., Zhang, S., Xing, J., Sun, Y., Ji, D., Chan, C. K., Gao, J., and McElroy, M. B.: Contribution of Particulate Nitrate Photolysis to Heterogeneous Sulfate Formation for Winter Haze in China, Environ. Sci. Technol. Lett., 7, 632-638, 10.1021/acs.estlett.0c00368, 2020.

755    Zhou, M., Nie, W., Qiao, L., Huang, D. D., Zhu, S., Lou, S., Wang, H., Wang, Q., Tao, S., Sun, P., Liu, Y., Xu, Z., An, J., Yan, R., Su, H., Huang, C., Ding, A., and Chen, C.: Elevated formation of particulate nitrate from N2O5 hydrolysis in the Yangtze River Delta region from 2011 to 2019, Geophys. Res. Lett., n/a, e2021GL097393, https://doi.org/10.1029/2021GL097393, 2022.

760

## Tables and Figures

**Table 1.** Model performance for meteorological parameters for January, April, July, October and the annual average of 2017 in the entire YRD region. The values that do not meet the criteria are denoted in bold.

| Parameters | Statistic(benchmarks) | January | April | July | October | Annual |
|---|---|---|---|---|---|---|
| T2(°C) | MB ($\leq \pm 0.5$) | **1.56** | **1.04** | **0.67** | **1.98** | **1.31** |
|  | RMSE | 1.99 | 1.76 | 1.57 | 2.24 | 1.89 |
|  | IOA ($\geq 0.8$) | 0.89 | 0.93 | 0.85 | 0.89 | 0.89 |
|  | R | 0.94 | 0.93 | 0.85 | 0.95 | 0.92 |
| RH(%) | MB | -6.96 | -10.70 | -9.06 | -5.98 | -8.17 |
|  | RMSE | 9.73 | 13.14 | 10.91 | 8.02 | 10.45 |
|  | IOA | 0.88 | 0.83 | 0.72 | 0.82 | 0.81 |
|  | R | 0.90 | 0.91 | 0.88 | 0.87 | 0.89 |
| WD(°) | MB ($\leq \pm 10$) | **-12.78** | -0.92 | **12.26** | **-24.42** | -6.46 |
|  | RMSE | 37.68 | 36.04 | 26.61 | 55.85 | 39.05 |
|  | IOA | 0.88 | 0.89 | 0.88 | 0.76 | 0.85 |
|  | R | 0.85 | 0.82 | 0.85 | 0.70 | 0.81 |
| WS(m/s) | MB ($\leq \pm 0.5$) | **0.61** | **0.76** | **1.03** | **0.69** | **0.77** |
|  | RMSE ($\leq 2.0$) | 0.82 | 1.06 | 1.31 | 0.96 | 1.04 |
|  | IOA ($\geq 0.6$) | 0.84 | 0.71 | 0.65 | 0.82 | 0.76 |
|  | R | 0.89 | 0.75 | 0.75 | 0.88 | 0.82 |

765     Notes: The following equations of MB, RMSE and IOA are defined in Table S4. The benchmarks are suggested by Emery and Tai (2001).

Atmospheric Chemistry and Physics Discussions

767 **Table 2.** Model performance of major pollutants for the full year of 2017 in five representative YRD cities [a].

| [b] Pollutants | Shanghai | | | | Nanjing | | | | Hefei | | | | Hangzhou | | | | Changzhou | | | |
|---|---|---|---|---|---|---|---|---|---|---|---|---|---|---|---|---|---|---|---|---|
| | [c] NMB | NME | MB | R | NMB | NME | MB | R | NMB | NME | MB | R | NMB | NME | MB | R | NMB | NME | MB | R |
| MDA8 $O_3$ | -0.01 | 0.20 | -1.07 | 0.88 | **0.17** | 0.28 | 18.59 | 0.76 | **0.17** | 0.24 | 17.23 | 0.81 | **0.25** | 0.31 | 26.60 | 0.80 | **0.19** | **0.26** | 19.85 | 0.84 |
| $NO_2$ | -0.05 | 0.23 | -1.89 | 0.71 | -0.07 | 0.26 | -3.20 | 0.50 | -0.11 | 0.26 | -5.21 | 0.67 | -0.25 | 0.34 | -10.37 | 0.51 | -0.07 | 0.24 | -2.67 | 0.56 |
| $SO_2$ | -0.38 | 0.43 | -4.61 | 0.66 | 0.12 | 0.45 | 1.83 | 0.32 | 0.01 | 0.36 | 0.18 | 0.75 | -0.28 | 0.40 | -3.15 | 0.46 | 0.09 | 0.34 | 1.54 | 0.48 |
| CO | -0.38 | 0.40 | -0.29 | 0.67 | -0.17 | 0.33 | -0.17 | 0.45 | -0.22 | 0.26 | -0.19 | 0.76 | -0.30 | 0.34 | -0.25 | 0.55 | 0.06 | 0.25 | 0.05 | 0.64 |
| $PM_{2.5}$ | -0.08 | 0.30 | -2.80 | 0.73 | 0.28 | 0.44 | 10.29 | 0.75 | **0.41** | **0.51** | 21.42 | 0.76 | 0.05 | 0.31 | 1.88 | 0.69 | 0.25 | 0.37 | 10.59 | 0.78 |
| $NO_3^-$ | -0.49 | 0.63 | -3.25 | 0.70 | | | | | 0.07 | 0.65 | 0.32 | 0.59 | 0.11 | 0.79 | 0.64 | 0.43 | -0.36 | 0.58 | -3.34 | 0.56 |

768 Notes: [a] The year of 2017 includes the four typical months (January, April, July, and October). [b] MDA8 $O_3$, $NO_2$, $SO_2$ and $PM_{2.5}$ units (μg/m³), CO units (mg/m³).

769 [c] The equations of NMB, NME, MB and R are found in Table S4. The values that do not meet the criteria are highlighted in bold.

770 The recommended benchmarks for MDA8 $O_3$, 24-h $PM_{2.5}$ and $NO_3^-$ are suggested by Emery et al. (2017) and Huang et al. (2021).

771

**Table 3.** Model performance for production rates (ppb/h) and daily contributions in percentage of the major production pathways (%) for the four seasons of 2017 in five representative YRD cities.

| Selected cities | Seasons | $TNO_3$ | $OH\ NO_2$ | $HET\ N_2O_5$ | $OH\ NO_2$ (%) | $HET\ N_2O_5$ (%) | Others (%) |
|---|---|---|---|---|---|---|---|
| Shanghai | Winter | $0.31 \pm 0.13$ | $0.21 \pm 0.18$ | $0.09 \pm 0.06$ | 69.3% | 28.4% | 2.2% |
| | Spring | $0.65 \pm 0.35$ | $0.52 \pm 0.43$ | $0.10 \pm 0.09$ | 81.8% | 15.3% | 2.9% |
| | Summer | $1.09 \pm 0.68$ | $0.90 \pm 0.80$ | $0.13 \pm 0.15$ | 82.9% | 12.2% | 4.9% |
| | Autumn | $0.28 \pm 0.22$ | $0.24 \pm 0.24$ | $0.03 \pm 0.03$ | 86.9% | 11.1% | 2.0% |
| Nanjing | Winter | $0.38 \pm 0.13$ | $0.23 \pm 0.20$ | $0.14 \pm 0.11$ | 59.2% | 36.1% | 4.7% |
| | Spring | $0.65 \pm 0.29$ | $0.48 \pm 0.40$ | $0.14 \pm 0.12$ | 73.1% | 21.4% | 5.4% |
| | Summer | $0.83 \pm 0.41$ | $0.62 \pm 0.55$ | $0.15 \pm 0.17$ | 74.7% | 17.9% | 7.4% |
| | Autumn | $0.50 \pm 0.25$ | $0.35 \pm 0.32$ | $0.13 \pm 0.11$ | 69.7% | 25.4% | 4.9% |
| Hefei | Winter | $0.38 \pm 0.13$ | $0.26 \pm 0.18$ | $0.10 \pm 0.07$ | 66.9% | 27.1% | 6.0% |
| | Spring | $0.63 \pm 0.24$ | $0.49 \pm 0.30$ | $0.10 \pm 0.09$ | 78.5% | 16.5% | 5.0% |
| | Summer | $0.66 \pm 0.26$ | $0.54 \pm 0.30$ | $0.07 \pm 0.08$ | 81.7% | 10.4% | 7.9% |
| | Autumn | $0.48 \pm 0.18$ | $0.35 \pm 0.24$ | $0.11 \pm 0.08$ | 72.5% | 21.8% | 5.7% |
| Changzhou | Winter | $0.41 \pm 0.15$ | $0.29 \pm 0.20$ | $0.11 \pm 0.08$ | 68.9% | 26.8% | 4.3% |
| | Spring | $0.64 \pm 0.25$ | $0.48 \pm 0.31$ | $0.13 \pm 0.12$ | 74.9% | 20.9% | 4.2% |
| | Summer | $0.70 \pm 0.27$ | $0.55 \pm 0.31$ | $0.10 \pm 0.13$ | 78.7% | 14.3% | 7.0% |
| | Autumn | $0.46 \pm 0.19$ | $0.36 \pm 0.24$ | $0.08 \pm 0.07$ | 77.6% | 18.3% | 4.1% |
| Hangzhou | Winter | $0.43 \pm 0.15$ | $0.26 \pm 0.21$ | $0.15 \pm 0.12$ | 59.7% | 35.5% | 4.8% |
| | Spring | $0.57 \pm 0.24$ | $0.40 \pm 0.33$ | $0.13 \pm 0.12$ | 70.5% | 23.3% | 6.2% |
| | Summer | $0.47 \pm 0.23$ | $0.36 \pm 0.29$ | $0.05 \pm 0.05$ | 76.4% | 10.7% | 12.9% |
| | Autumn | $0.46 \pm 0.26$ | $0.34 \pm 0.32$ | $0.10 \pm 0.09$ | 73.8% | 21.3% | 4.9% |

772
773
774

Atmospheric
Chemistry
and Physics
Discussions

775 **Table 4.** Comparison of contributions of major nitrate formation pathways in China and others regions [a].

| References | Methods [b] | Study seasons | Year | Study regions | $NO_3^-$ formation pathways [c] | Time metric | Contribution (%) |
|---|---|---|---|---|---|---|---|
| (Li et al., 2021b) | WRF-Chem | Warm (Aug –Sep) | 2016 | NCP, YRD | $OH+NO_2$ (layer 1) | season-mean | 60-92% |
| | | Cold (Nov-Dec) | | | HET $N_2O_5$ (layer 1) | | 8-40% |
| (Qu et al., 2021) | WRF-CMAQ PA | Transition season (Oct-Dec) | 2015 | PRD | $OH+NO_2$ (layers 1-4) | day-mean | 92-96% |
| | | | | | HET $N_2O_5$ (layers 1-4) | night- mean | 64-72% |
| (Chuang et al., 2022) | WRF-CMAQ PA | Transition season (Mar - Apr) | 2017 | Taiwan | $OH+NO_2$ | day-mean | > 90% |
| | | | | | HET $N_2O_5$ | night- mean | 30-90% |
| (Wu et al., 2021) | WRF-Chem; Nitrogen Isotopes | Cold (Dec-Jan) | 2017 | Xi'an | HET $N_2O_5$ (surface) | season-mean | 13-35 % |
| (Chan et al., 2021) | GEOS-Chem; Isotope tracing | Cold | 2014-15 | NCP | $OH+NO_2$&HET $N_2O_5$ (surface) | season-mean | 34 % & 45 % |
| (Fu et al., 2020) | WRF-CMAQ PA | Cold (Dec) | 2017 | NCP | $OH+NO_2$ (HET $N_2O_5$) 10 layers | season-mean | 43% (44%) |
| (Liu et al., 2020a) | WRF-Chem | Cold (Dec) | 2016 | NCP | HET $N_2O_5$ (surface) | haze-mean | 52 % |
| | | | | | HET $N_2O_5$ (PBL) | night (day) | 83% (10%) |
| (Zhang et al., 2021) | Nitrogen &Oxygen Isotopes | Cold (Nov-Jan) | 2017-18 | Nanchang | HET $N_2O_5$ (surface) | season-mean | 60% |
| (Fan et al., 2021) | Nitrogen &Oxygen Isotopes | Warm and Cold | 2016-17 | Beijing | $OH+NO_2$&HET $N_2O_5$ (260 m) | Clean days | 20% (80%) |
| (Luo et al., 2020a) | Nitrogen &Oxygen Isotopes | Spring(Mar-May) | 2013 | Beijing | $OH+NO_2$ (surface) | Clean days | 24-50% |
| | | | | | $OH+NO_2$ (surface) | Polluted days | 11-47% |
| (Luo et al., 2020b) | Nitrogen &Oxygen Isotopes | Four seasons | 2018 | Nanchang | $OH+NO_2$ (HET $N_2O_5$) | season-mean | 12-59% (67-89%) |
| (Fan et al., 2020) | Nitrogen &Oxygen Isotopes | Cold (Nov-Dec) | 2018 | Beijing | HET $N_2O_5$ | haze period | 64% |
| (He et al., 2020) | Nitrogen &Oxygen Isotopes | Warm and Cold season | 2016 | Shanghai | $OH+NO_2$ (warm) | season-mean | 84-92% |
| | | | | | $OH+NO_2$ (cold) | | 48-74% |
| (Wang et al., 2019) | Nitrogen &Oxygen Isotopes | Warm and Cold season | 2014 | Beijing | $OH+NO_2$ | annual-mean | 32 ± 10% |
| | | | | | HET $N_2O_5$ | annual-mean | 68 ± 23% |
| (He et al., 2018) | Nitrogen isotopic | Cold (Oct-Jan) | 2014 | Beijing | HET $N_2O_5$ | night- haze | 56-97 % |
| (Chen et al., 2020) | Field determination; Box model | Cold (Nov-Dec) | 2016-17 | Beijing | $OH+NO_2$& HET $N_2O_5$ (240 m) | haze period | 74-76% & 34% |
| (Zang et al., 2022) | Field observations; Box model | Cold (Dec-Feb) | 2018-19 | Shanghai (urban | $OH+NO_2$&HET $N_2O_5$ (surface) | haze period | 69% & 29% |

Atmospheric
Chemistry
and Physics
Discussions

Open Access
EGU

| Reference | Method | Season | Year | Region | Pathway | Mean | Contribution |
|---|---|---|---|---|---|---|---|
| (Womack et al., 2019) | Box model | Cold (Dec) | 2016-17 | Salt Lake Valley & suburban areas) | $OH+NO_2$ & HET $N_2O_5$ (surface) | haze period | 63% & 35% |
| | | | | | HET $N_2O_5$ (RL) | season-mean | 43% |
| (Vrekoussis et al., 2004) | Field determination, Box model | Summer(Jul-Aug) | 2001 | South-East Europe | HET $N_2O_5$ (surface) | season-mean | 21% |
| (Kim et al., 2014) | WRF-CMAQ PA | Cold (Dec) | 2009 | The Great Lakes | $OH+NO_2$ & HET $N_2O_5$ (surface) | season-mean | 28% & 57% |
| (Shah et al., 2018) | GEOS-Chem | Cold (Feb-Mar) | 2015 | Eastern US | $OH+NO_2$ & HET $N_2O_5$ (surface) | season-mean | 36% & 62% |
| (Alexander et al., 2020) | GEOS-Chem; Oxygen Isotopes | Four seasons | 2000-15 | Global | $OH+NO_2$ (below 1 km) | annual-mean | 41-42% |
| | | | | | HET $N_2O_5$ (below 1 km) | | 28-41% |

776     Notes: [a] The above studies are conducted in the major regions and megalopolises of China (the North China Plain (NCP), Yangtze River Delta (YRD), Pearl River

777     Delta (PRD)), the United States, and the Global region. The comparison serves to quantify the relative contribution of two main nitrate formation pathways in different

778     seasons. [b] Methods include the 3-D CTMs, nitrogen and oxygen isotopes analysis, field determination, and box model. [c] Surface represents the surface layer.
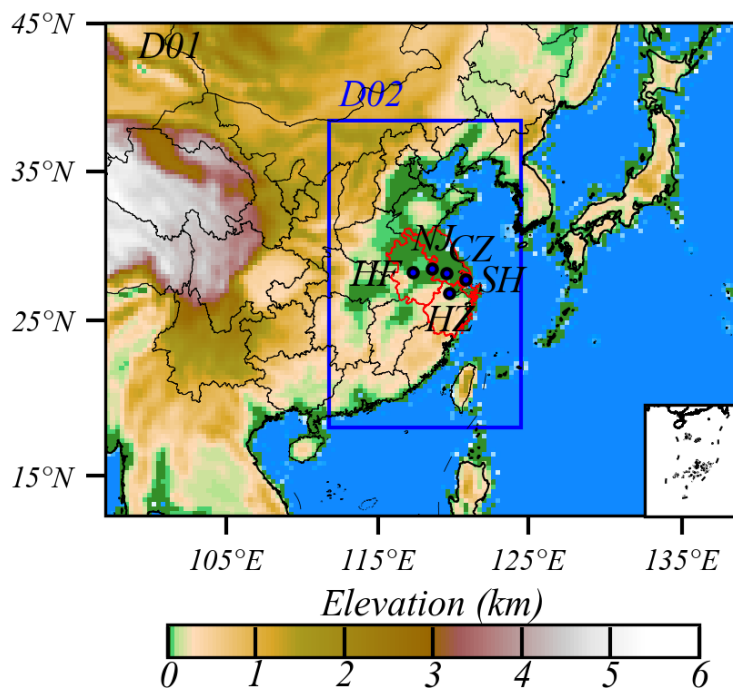
**Fig 1.** Entire YRD region as the target region (marked as red) in two nested simulation domains (36 and 12 km resolutions), and location of five representative YRD cities used in modeling evaluations in the d02 modeling domain.

Atmospheric
Chemistry
and Physics
Discussions

Open Access

EGU
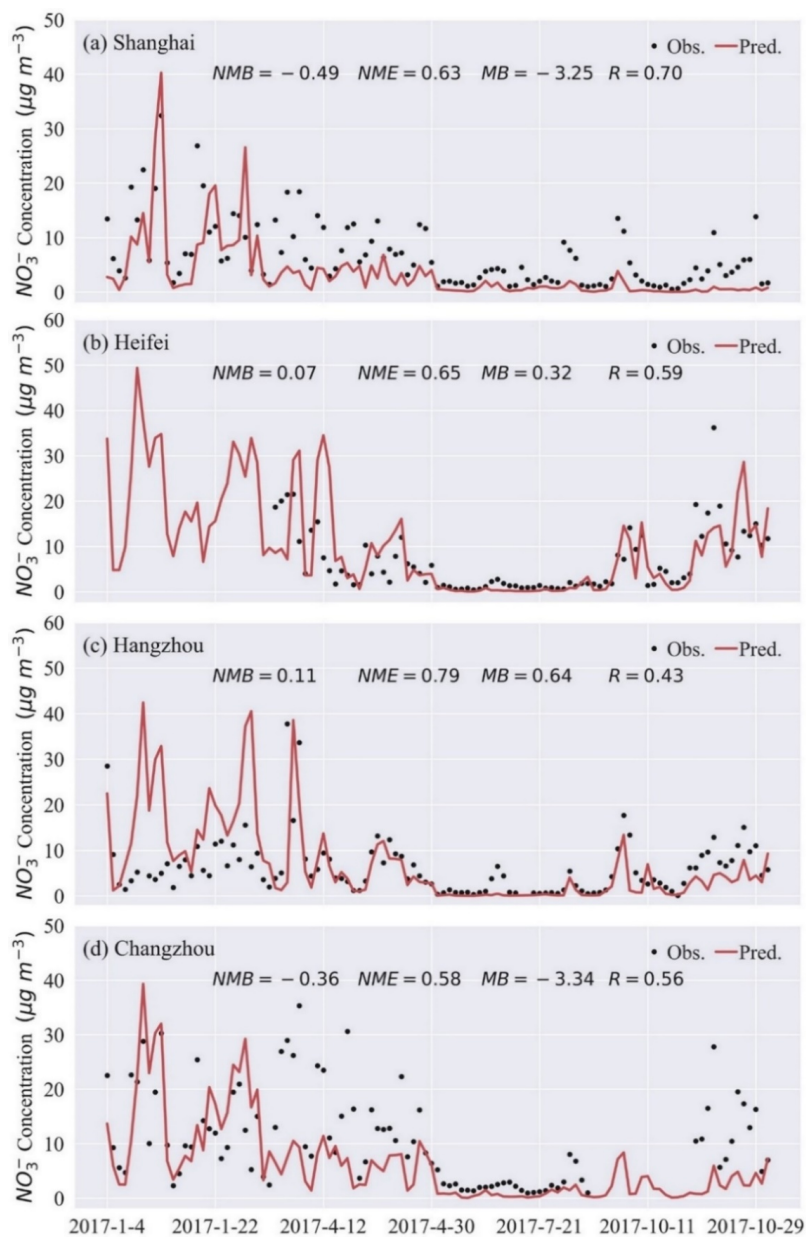


**Fig 2.** Time series of predicted (red) and observed (black) daily NO₃⁻ concentrations in four atmospheric environment supersites (a–d) in January, April, July, and October 2017.
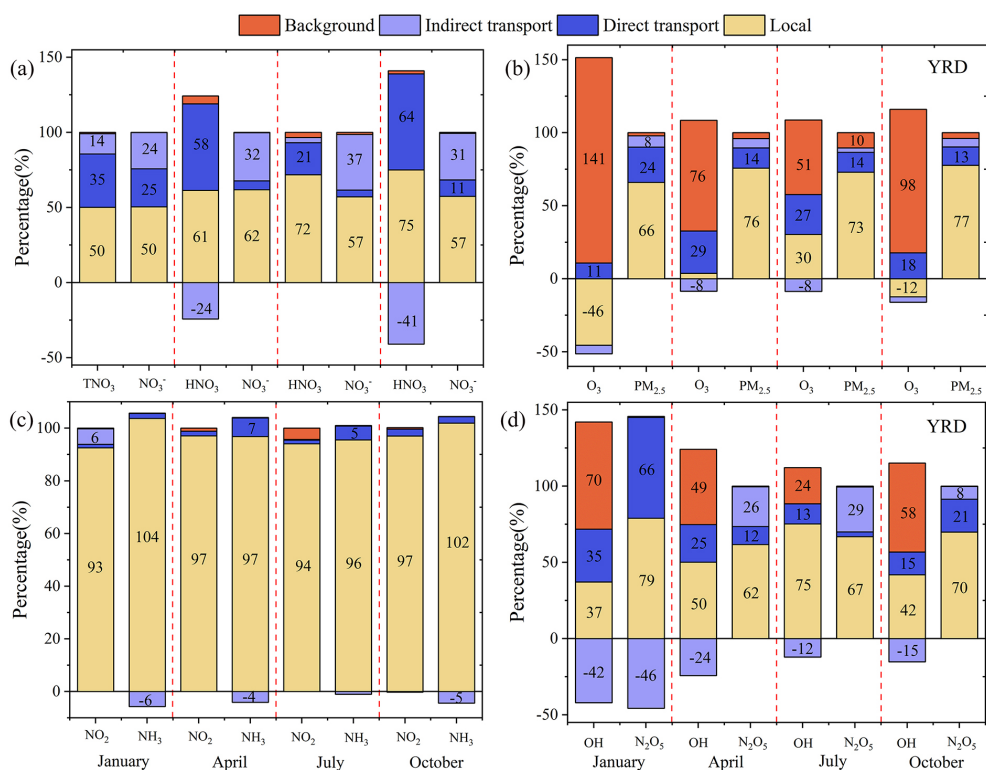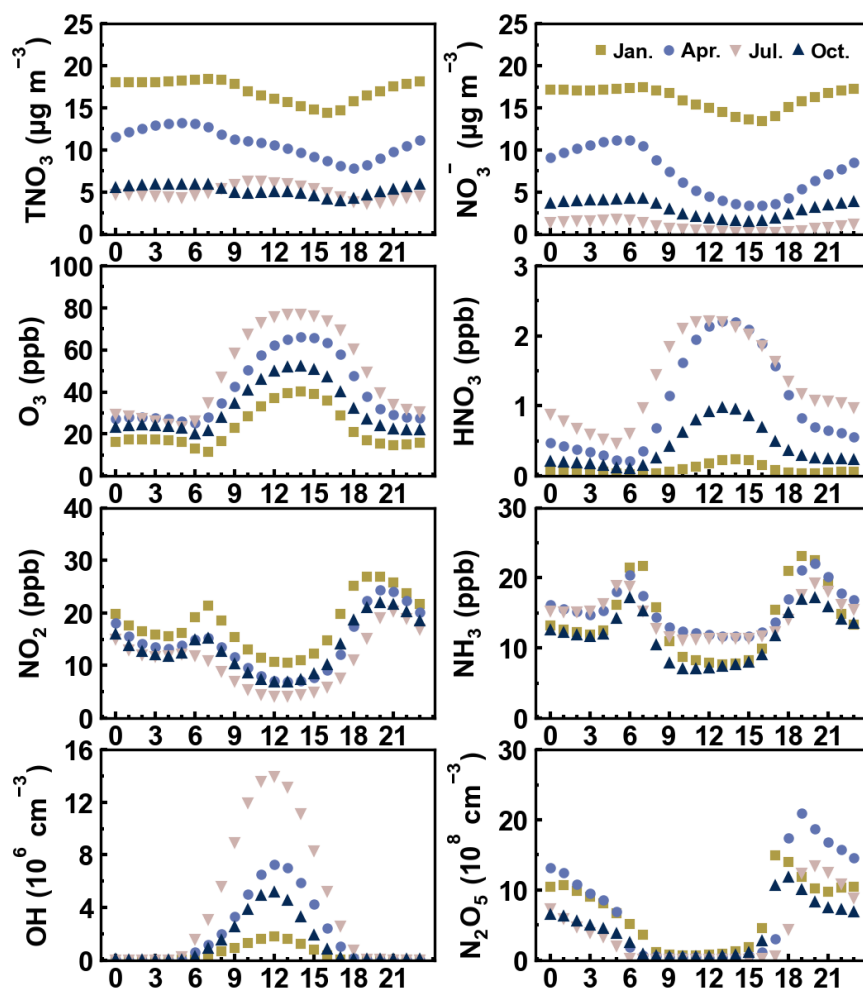
**Fig 3.** (a–d) Contributions of Background, Local, Indirect, and Direct transport to nitrate-related species in four months of 2017 for the entire YRD region.

Notes: Nitrate-related species represent $NO_3^-$, $HNO_3$, $PM_{2.5}$, $O_3$, $NO_2$, $NH_3$, OH, and $N_2O_5$. The contributions of $HNO_3$ in January 2017 are shown in Fig. S6.

**Fig 4.** Monthly diurnal variations of three nitrate-phases ($NO_3^-$, $HNO_3$, and $TNO_3$), major nitrate-precursors ($O_3$, $NO_2$, and $NH_3$) and major atmospheric oxidants (OH and $N_2O_5$) for the entire YRD region under the base scenario. The X axis marks each hour of the day (Beijing time).
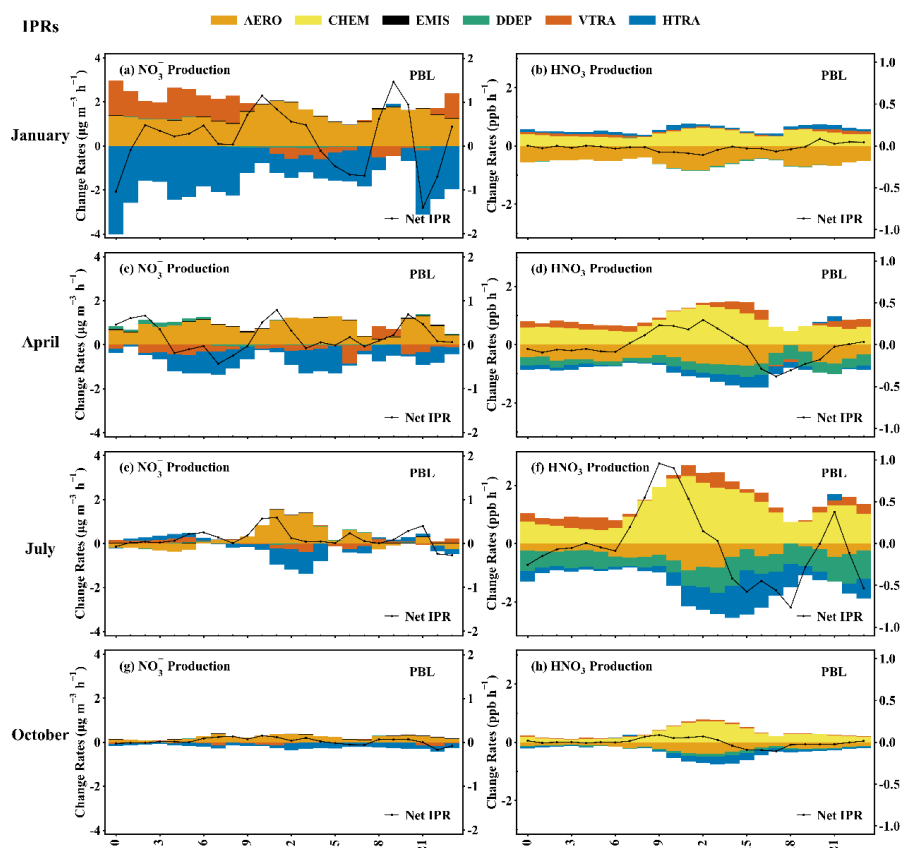
**Fig 5.** Diel variations in physical and chemical processes rates of $NO_3^-$ and $HNO_3$ production (a–h) within the PBL in Shanghai. Black line represents the net IPR value for each hour of the day; its value scale is on the right Y axis.

802

803
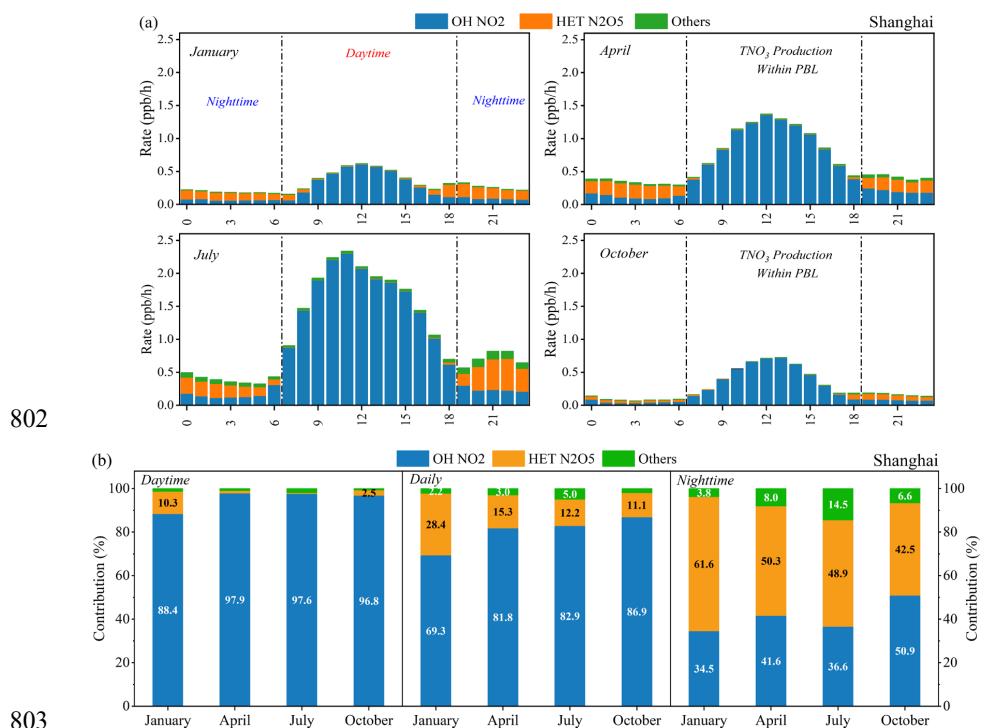


**Fig 6.** (a) Mean diurnal variations of TNO$_3$ production rates in different pathways in
2017 in Shanghai. (b) Average potential contribution of OH + NO$_2$, HET N$_2$O$_5$ and
Others pathways to TNO$_3$ chemical production in Shanghai within the PBL under base
case simulation.

Notes: Daytime (7:00–18:00), Nighttime (19:00–6:00). OH + NO$_2$ and HET N$_2$O$_5$ pathways are
noted as "OH NO2" and "HET N2O5" in Figs.6 and 7.

804
805
806
807
808
809
810
811
812
813
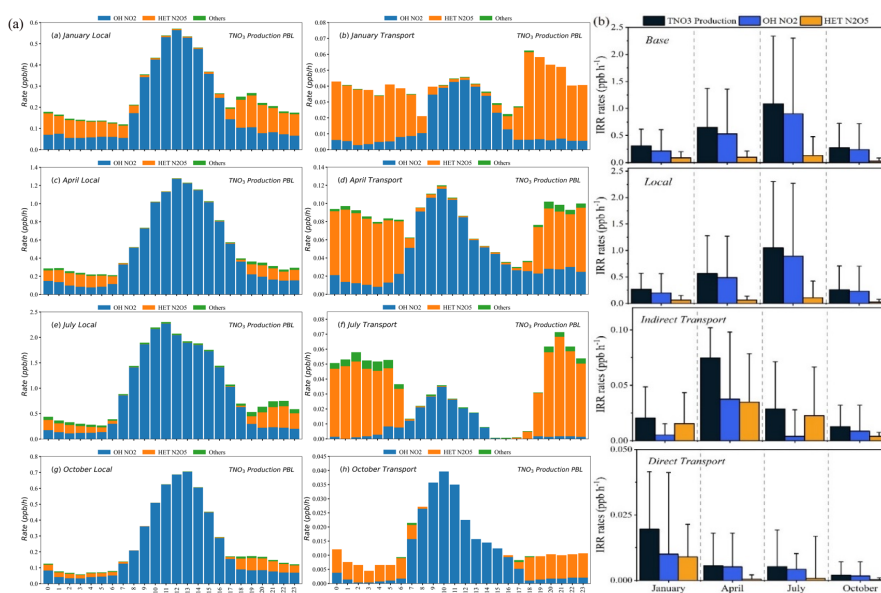
**Fig 7.** (a) Mean diurnal variations of TNO$_3$ production rates in major pathways from the local and transport (sum of indirect and direct transport) contributions. (b) Total IRRs rates of TNO$_3^-$ production rates in the base case and from the local and transport contributions within the PBL. The error bar indicates one standard deviation.